8-2018

A Quantitative Analysis of Calcareous Nannofossils Across a Late Oligocene Paleolatitude Transect of the North Atlantic Ocean

William Barrett Clark
University of Nebraska-Lincoln, wclark38@gmail.com

A QUANTITATIVE ANALYSIS OF CALCAREOUS NANNOFOSSILS ACROSS A LATE OLIGOCENE PALEOLATIUDE TRANSECT OF THE NORTH ATLANTIC OCEAN

By

William Barrett Clark

A THESIS

Presented to the Faculty of

The Graduate College at the University of Nebraska

In Partial Fulfillment of Requirements

For the Degree of Master of Science

Major: Earth & Atmospheric Sciences

Under the Supervision of Professor David K. Watkins

Lincoln, Nebraska

August 2018

A QUANTITATIVE ANALYSIS OF CALCAREOUS NANNOFOSSILS ACROSS A LATE OLIGOCENE PALEOLATIUDE TRANSECT OF THE NORTH ATLANTIC OCEAN

William Barrett Clark, M.S.

University of Nebraska, 2018

Advisor: David K. Watkins

Samples from ODP Sites 926, 628, 563, U1406, 647, and 918, were analyzed quantitatively across a paleolatitude transect of the North Atlantic Ocean to determine the paleolatitudinal distribution of calcareous nannofossils in the Late Oligocene and the effects of that distribution on biostratigraphic resolution. Detrended Correspondence Analysis (DCA), a Temperature index (TI), and the Shannon Diversity Index (H), were used to examine the paleoenvironmental gradients which exerted the most control over the distribution of species and their abundances. The temperature index correlates significantly to the first axis of the DCA, suggesting that thermal controls were the most important factor in the distribution of Late Oligocene nannofossils in the North Atlantic. Shannon Diversity and the percent abundance of the taxon *Reticulofenestra minuta* correlates significantly to DCA 2, suggesting that surface water mass fertility was an important secondary controlling factor during the Late Oligocene. A biochronological analysis utilizing Unitary Associations (UA) divided the assemblage into 6 UAs, correlating with the biostratigraphic scheme of Agnini et al. (2014). UA 3 and UA 4, defined by the base of *Sphenolithus calyculus*, was not used in the Agnini et al. (2014) biozones, and offers an additional bioevent for the Upper Oligocene. The absence of UA 5 at Hole 926B reveals a disconformity that was not identified previously. The zonation scheme of Bergen et al. (2017) which utilizes *S. calyculus*, and Agnini et al. (2014) cannot be accurately applied to the

North Atlantic Ocean north of 53° latitude. The best biostratigraphic resolution in the Late Oligocene North Atlantic is restricted to the upper mid latitudes Sites 628, 563, and U1406. These latitudes, from 27-40˚, represent the warm gyre center and the temperate gyre perimeter.

Acknowledgements:

Samples for this study were obtained from the Deep Sea Drilling Project (DSDP) and the Ocean Drilling Program (ODP). DSDP and ODP are sponsored by the National Science Foundation (NSF) and participating countries under the management of Joint Oceanographic Institutions (JOI), Inc. I would like to thank my committee members, Drs. Tracy Frank and David Harwood, for their excellent instruction and improvements for this thesis, colleague Shamar Chin, for her morale support and friendship, and Drs. Murlene and Raymond Clark for their boundless encouragement, and positive advice. I would especially like to thank my advisor, Dr. David Watkins, for his invaluable expertise, and help in guiding me through this project.

TABLE OF CONTENTS: **PAGE:**

LIST OF FIGURES **PAGE:**

LIST OF TABLES **PAGE**

1.0 Introduction:

The Late Oligocene was a time of transition in the North Atlantic Ocean, when colder sea surface temperatures, coupled with corrosive deep-water masses, created a stressed environment for calcareous nannoplankton (Kennett, 1982, Pekar et al. 2006). Nannofossil populations were forced to adapt rapidly to a paleoceanographic restructuring (Pekar et al., 2002; Miller et al., 1987; Stoker et al., 2002; Heydt and Dijkstra, 2006). There are few studies which utilize quantitative methodology to analyze and constrain paleoecological changes in calcareous nannofossil distribution in the Late Oligocene North Atlantic Ocean. Modern biostratigraphic schemes for the Late Oligocene North Atlantic are based on a synthesis of data from the Equatorial Pacific (Blaj et al. 2009; Bown and Dunkley-Jones 2012), Southern Atlantic (Wise and Wind, 1983; Agnini et al., 2014), and the Atlantic Equatorial Divergence (Shackleton et al. 1999). This study utilizes quantitative paleoecological and biostratigraphic analyses of calcareous nannofossil assemblages to constrain their paleoceanographic distribution, and the effect of that distribution on regional biostratigraphy of the North Atlantic Ocean. Abundances of dominant taxa have been correlated to species diversity, and a temperature index to better examine the primary controls acting on the Late Oligocene paleoenvironment. The primary paleoecological, and tectonic drivers of North Atlantic paleoceanography are examined further, to assess potential controls on Late Oligocene paleoproductivity.

1.1 Paleoceanography of the Oligocene North Atlantic Ocean:

During the Early Oligocene, at 33 Ma, the convergent plate movements of Greenland and northeastern North America terminated (Jaspen et al., 2005). Although

Greenland had ceased movement, there were several compressional faults along its western margin which facilitated pulses of uplift (Jaspen et al., 2006). This uplift created a planation surface within the Labrador Basin during the Oligocene. Tectonic pulses resulted in the removal of sediments along the West Greenland Margin, which were deposited into the Southern Labrador Sea, with reburial in the Early Miocene (Jaspen et al., 2005). Micropaleontological studies within the West Greenland Margin and the North Labrador Sea have noted several unconformities within assemblages of dinoflagellate cysts (Piasecki, 2003). These unconformities coincide with tectonic uplifting and denote a 40 m.y. time gap from the Middle Eocene to the Early Miocene (Piasecki, 2003).

The start of the Late Oligocene at 26 Ma included the earliest closure of two primary seaways that controlled water input into and output from the North Atlantic. Due to the collision of the African/Arabian and Iranian/Eurasian plates the Tethys Seaway shallowed, partially halting warm nutrient rich water inflow from the Indian Ocean into the North Atlantic (Heydt and Dijkstra, 2006; Reuter et al., 2009). Simultaneously, the Panama Seaway underwent narrowing, significantly reducing the flow of cooler Pacific waters into the Caribbean and by 25 Ma, the flow of the Central American Seaway was disrupted (Montes et al., 2012). The loss or reduction of these connections led to the permanent cessation of the Circum-equatorial Current (Montes et al., 2012). In the Southern Ocean, complete deep-water separation of Antarctica and South America occurred at the Drake Passage (Pekar et al 2006; Cramer et al. 2009). This may have provided the tectonic impetus to restrict flow of the Panamanian Seaway as South America moved northward (Pekar et al. 2006). The thermal isolation of Antarctica may have strengthened the volume of Antarctic bottom water, which traveled northward

(Scher and Martin, 2006; Livermore et al. 2005; Pfuhl and McCave, 2005); however, Pekar et al., (2006) indicate that a deep water opening of the Drake Passage would have isolated the Antarctic bottom water to the higher latitudes of the Southern Ocean.

In the northeastern Atlantic, at 26 Ma, both the Iceland-Faroe Ridge and the Greenland-Scotland Rise underwent drowning and subsidence, which was coincident with sizable uplift on the Western Greenland Margin (Japsen, 2005; Stoker et al., 2002). The subsidence of both of these barriers established a deep-water connection between the North Atlantic Ocean and the Arctic Sea. According to Stoker et al. (2002) the sudden onset of these tectonic events led to a high velocity deep-water erosional current which scoured the bottom of the eastern North Atlantic. With this connection, it is possible a proto - North Atlantic Deep Water Mass was established. At this time, the primary locus of deep-water production was still in the North Pacific (Pekar et al., 2006). The volume of any NADW would have been much lower than it is today and may have acted as intermediate water in certain parts of the water column (Heydt and Dijkstra, 2006).

The Gulf Stream was first established, at least, by the Maastrichtian and strengthened in the northwestern Atlantic near the Florida Straits and Blake Nose during the Middle-Late Eocene (Pinet and Popenoe 1985, Watkins and Self-Trail, 2005). The location of the Gulf Stream current is variable, shifting in response to different paleoenvironmental circumstances. Sea level rise at the Blake Nose during the Eocene pushed the Gulf Stream south and west (Pinet and Popenoe, 1985). Warmer SSTs and stronger wind currents can shift the Gulf Stream north and east, while colder SSTs can push the current south and west (Frankignoul et al. 2001).

The equatorial Atlantic today is under the influence of mixing currents from the South and North Atlantic divergence zone, as well as increased westward transport from the Gulf Stream. Divergence waters from the South Atlantic are fed into the North Atlantic through the North Brazil Coastal Current into the North Equatorial Current, intersecting with the western and northern flow of the Gulf Stream (Gibbs et al., 2004).

2. Materials and Methods

2.1 Materials:

Upper Oligocene core material is rare within the North Atlantic Ocean due to incomplete core recovery, intervals of poor preservation, and disconformities within the sections. For this study, the best available ODP, IODP, and DSDP sites (Fig. 1) were selected for their relatively complete and well-preserved material across sixty degrees of latitude including, from south to north, Holes 926B (Ceara Rise), 628 (Florida Straits), 563 (Mid Oceanic Ridge), U1406 (South Newfoundland Ridge), 647A (South Labrador Sea), and 918D (Greenland-Scotland Rise). Sediments from Holes 926B, U1406, and 918D were collected using Advanced Piston Coring (APC) techniques, while Hydraulic Piston Coring (HPC) and Rotary Coring were used to collect Hole 628 and Holes 563 and 647A, respectively.

ODP Leg 154, Site 926B

ODP Leg 154 Hole 926B is located in the equatorial Atlantic Ocean at 3°43.148'N, 42°54.507'W. Hole 926B lies at a water depth of 3598 m and is at the southernmost point of an ODP transect drilled along the Ceara Rise (Curry et al., 1995). Thirty-five samples were obtained from Cores 50X to 61X (469.9-571 mbsf). Dominant

lithology is carbonate nannofossil ooze, with a section thickness of 101.1 m. The Upper Oligocene section is complete with no observed disconformity and represents a continuous Late Oligocene interval from 26.9 to 23.03 Ma.

ODP Leg 101, Site 628

ODP Leg 101 Site 628 is located in the western Atlantic Ocean at 27°31.85'N, 78°18.95'W, on the northern slope of Little Bahama Bank at a water depth of 959 m. Thirty samples were obtained from Cores 16H to 24X (137.9 – 220 mbsf). Dominant lithology consists of bioturbated carbonate oozes and chalks with sporadic horizons of pyrite-rich material. The thickness of the Upper Oligocene section is measured at 82.1 m. A disconformity, as explained by Watkins and Verbeek (1988) extends from the Lower Miocene to the Uppermost Oligocene located above Core 16H.

DSDP Leg 82, Site 563

DSDP Leg 82 Site 563 is located in the Central Atlantic Ocean at 33°38.53'N, 43°46.04'W, on the western slope of the Mid Atlantic Ridge at a water depth of 3796 m. Thirty-seven samples were obtained from Cores 16R to 19R (301.8 – 330.6 mbsf). Dominant lithology is composed of pelagic chalk, with layers of alternating nannofossil and foraminifera oozes. The thickness of the section is measured at 28.8 m. Site 563 has a complete Upper Oligocene calcareous nannofossil succession, based on the biostratigraphic analysis of Parker, (1985). Miller et al. (1985) has noted a possible disconformity between Cores 17 and 18.

IODP Leg 342, Hole U1406

IODP Leg 342 Hole U1406A is located in the Central Atlantic Ocean at 40°21.0′ N, 51°39.0′ W, near the Southeast Newfoundland Ridge, at a water depth of 3798.9 m. Forty samples were obtained from Cores 9H to 18H (78.9 – 163.6 mbsf). Dominant lithology is light yellow, light greenish gray to greenish-grey nannofossil ooze, with common green layers of glauconite and chlorite disseminated throughout. The section has an average 40% weight content of $CaCO_3$, and a thickness measured at 84.7 m. Based on an Age-Depth model developed by Norris et al. (2014) there is a hiatus in the Upper Oligocene from 26-28 Ma. The shipboard scientific report places the base of *Sphenolithus ciperoensis* at 29.62 Ma, which differs from the tuned age of Shackleton et al. (1999) and Gradstein et al. (2012) by 2.72 m.y.

ODP Leg 105, Hole 647A

ODP Leg 105 Hole 647A is located in the Southern Labrador Sea at 53°19.876'N, 45°15.717'W, east of the northwest Atlantic Mid-Ocean Canyon, at a water depth of 3858.5 m. Seventeen samples, assigned to the Upper Oligocene, were utilized from Cores 14R to 16R (128.7 – 146.1 mbsf). The lithology of the section differs between two units: Unit Two in Core 14R, and Unit Three in Cores 15R-16R. Unit Two is dominated by a quartz-silt to clayey silt. Unit Three is dominated by a moderately to strongly bioturbated, greenish grey to light greenish grey, biogenic clay or clayey ooze. The thickness of a possible Upper Oligocene section is estimated at 17.4 m, based on an examination by Firth, (1989), who notes individual specimens of *S. ciperoensis* and *Sphenolithus delphix*, in Cores 105-647A-16R-3, 36-38 cm and 105-647A-19R-4, 14-16 cm, respectively. The boundary between the Lower and Upper Oligocene is estimated to be lower within the

section (Firth, 1989). A biostratigraphic synthesis formulated by Baldauf et al. (1989) suggests that only the CP17/CP18 boundary is represented based on diatom data as well as the simultaneous occurrence of *Sphenolithus predistentus* and *Sphenolithus distentus* at sample 105-647A-15R-1, 68-70 cm. According to an age assessment conducted by Baldauf et al. (1989), there is a 7 m.y. hiatus between the Lower Miocene and Lower Oligocene, which would preclude the presence of an Upper Oligocene section at this site.

ODP Leg 152, Hole 918D

ODP Leg 152 Hole 918D is located in the North Atlantic Ocean at 63°5.572'N, 38°38.334'W, on the upper continental rise of the Southeast Greenland Margin, at a water depth of 1868.2 m. Twenty-four samples were obtained from Cores 62R to 84R (869 – 1080.4 mbsf). Dominant lithology of this section is interbedded sands and nannofossil chalks with a section thickness measured at 211.4 m. Based on the biostratigraphic analysis of Wei (1998) the Upper Oligocene section of Site 918D contains abundant Late Oligocene background taxa, but no marker species such as, *S. ciperoensis* or *S. delphix*, were identified. The Upper Oligocene is proposed to be complete with no disconformity (Wei, 1998).

2.2 Methods:

A total of 189 samples were prepared using a modified form of the random gravitational settling technique developed by Geisen et al. (1999). A sample of known weight (10-20 mg) was suspended in 1 L solution of distilled water and surfactant (Alconox ™), which was adjusted to a pH within the range of 8.3 to 8.5 by the addition of NH_4OH. The solution was poured into a settling chamber containing a coverslip

affixed to a raised dais and was allowed to settle for 24 hours. The chamber was then slowly drained, and the coverslip air dried, and subsequently mounted on a slide.

Specimens were identified using an Olympus BX-51 light microscope under 1250x magnification, through crossed-polarized and plane-polarized light. Species abundances were calculated based upon a 600 specimen count per sample, which reflects abundance estimates within 4% of the population at a 95% confidence interval (Chang, 1967). In addition, three, north to south traverses consisting of 50 fields of view (FOV) each, were performed to identify rare species.

Specimen preservation was qualitatively assessed through a scheme proposed by Watkins and Bowdler (1984) according to the following criteria:

Good (G) – Specimens show no signs of secondary alteration. Identification is not impaired.

Moderate (M) – Specimens show signs of early secondary alteration such as etching or overgrowth. Identification is not overly impaired.

Poor (P) – Specimens show signs of advanced secondary alteration with profound etching and overgrowth. Identification is impaired, though possible.

Qualitative estimates of nannofossil abundance, also described according to the criteria of Watkins and Bowdler (1984), were applied using a magnification of 1250x instead of the published 1500x. This estimation is as follows:

Abundant (A) – 1-10 specimens per field of view.

Common (C) – One specimen per 2-10 fields of view.

Few (F) – One specimen per 11-100 fields of view.

Rare (R) – One specimen per 101-1000 fields of view.

Barren (B) – No specimens per 3-5 traverses of slide.

The Upper Oligocene section examined in this study is represented by the interval between the first occurrence of *S. ciperoensis* through the last occurrence of *S. delphix*, which is equivalent to Biozones CNO4 – CNM1 of Agnini et al. (2014; Fig. 1). The location of the Oligocene-Miocene boundary will be interpreted here as the extinction of *S. delphix*.

The biochronology of this paleolatitude transect was developed based on the Geologic Time Scale 2012 (Gradstein et al., 2012). This timescale incorporates Oligocene biostratigraphy from several sources including the astronomically tuned timescale, developed by Shackleton et al. (1999) which uses biostratigraphic data from ODP Leg 154. The geologic time scale of Gradstein et al. (2012) places the first occurrence of *S. ciperoensis* at 26.9 Ma, and the last occurrence of *S. delphix* at 23.03 Ma. For higher latitude sites, such as Hole 647A and Hole 918D, the magnetostratigraphy established by the Norris et al. (2014) was applied in conjunction with Shackleton et al. (1999).

Data were analyzed using the PAST paleontological statistical program by Hammer et al. (2001). Detrended Correspondence Analysis (DCA) and Shannon Diversity analysis (H) were used to identify primary variance in the paleoecological distributions and paleoenvironmental stability. A DCA is an eigenvector extraction method whereby variables (species) have abundance peaks which correspond to optimal

conditions along an underlying environmental gradient. A DCA uses a similarity index to incorporate the probability of abundances of the variable. In PAST, Q-mode and R-mode are calculated simultaneously. Q-mode identifies the placement of the sample along the environmental gradient while R-mode identifies the placement of taxa.

In order to increase the statistical and quantitative potential of the dataset, three taxa of *Braarudosphaera* are identified in the range chart but are combined for the DCA.

The Shannon (H) is a diversity index which takes into account the number of individuals as well as the number of taxa (Hammer et al. 2001). A quantitative analysis using the % abundance of dominant taxa by sample was used in conjunction with the Shannon diversity index to correlate with possible paleoenvironmental influences through time.

In order to analyze sea surface temperatures at each site, a Temperature index (TI) was formulated. Modified from (Watkins and Self-Trail, 2005; Villa et al., 2014), the (TI) uses % abundance of nannofossil taxa whose paleoenvironmental preferences are for warm or cold sea surface temperatures. For warm taxa, all species of *Sphenolithus* and *Discoaster* were combined into their respective genera. For cold taxa, the species of *Coccolithus pelagicus* was utilized. The Temperature index formula is as follows:

$$TI = \left(\frac{\%\ warm\ taxa}{\%\ warm + \%\ cold\ taxa}\right) \times 100$$

TI = Temperature Index

% Warm taxa = % abundance of *Sphenolithus* + *Discoaster* per sample

% Cold taxa = % abundance of *Coccolithus pelagicus* per sample.

3. Results:

3.1 Detrended Correspondence Analysis (DCA):

The results of the DCA are represented in a plot of the samples, using DCA axis 1+2 (Fig. 2). Based on the DCA 1+2 plot the samples are separated into three groupings. Site 563 (orange) is separate and plots low on DCA 1 and high with respect to DC axis 2. Holes 926B (black), 628 (blue), and U1406 (red) are grouped closely and plotted high to axis 1 and low to axis 2. Finally, Holes 647A (green), and 918D (aqua) are plotted high to axis 1 and are loosely grouped together (Fig. 2). Samples 82-563-16R-3, 48-49 cm and 82-563-16R-4, 27-28 cm at site 563 are considered outliers.

3.2 Shannon Diversity (H) Index:

The Shannon diversity index incorporates species richness and evenness, with higher values indicating stable environments and lower values attributed to stressed or unstable environments. A graph of Shannon diversity was plotted through time at Holes 926B, 563, and U1406 (Fig. 3).

Hole 926B:

Shannon diversity at Hole 926B ranges from (1.0 to 2.37), with an average of 1.7. Shannon diversity increases through time from 26.7 to 24.5 Ma (Fig. 3). This increase starts at a low of 1.1 and terminates at a high of 2.1. From 24.5 to 23.11 Ma, the index stabilizes between 1.5 and 2.0 (Fig. 3).

Hole 563:

Shannon diversity at Site 563 ranges from (1.5 – 2.3), with an average of 2.0 (Fig. 3). Shannon diversity increases from 28.8 Ma to 25.2 Ma, or from a low of 1.8 to a high

of 2.3. From 25.2 to 24.5 Ma there is a slight decrease in diversity of 2.3 to 2.0, before the index stabilizes through 23.11 Ma at a range of (1.9 – 2.1) (Fig. 3).

Hole U1406:

Shannon diversity at Hole U1406 ranges from (1.3 to 1.89), with an average of 1.6 (Fig. 3). Shannon diversity decreases through time from 26.8 to 24.9 Ma, with a high of 1.6 to a low of 1.4. The index increases from 24.9 to 24 Ma, with 1.4 to 1.8. From 24 to 23.11 my, the index decreases from a high of 1.8 to a low of 1.5 (Fig. 3).

3.3 Abundance Trends of *Reticulofenestra minuta*:

The taxon of *R. minuta* at Holes 926B, 563, and U1406 was plotted with respect to age.

Hole 926B:

The taxon *R. minuta* has a decrease in % abundance within the interval between 26.7 to 25 Ma with a high value of 73% and a low of 25% (Fig. 4). *R. minuta* then has an increase in % abundance within the interval of 25 to 23.11 Ma, with a low of 25% and a high of 45%. There are two maxima within the *R. minuta* series, the first is found at 26.7 Ma with 73% and the second occurs at 23.8 Ma with 56% abundance (Fig. 4).

Site 563:

The taxon *R. minuta* has a decrease in % abundance within the interval of 28.8 to 25.6 Ma with a high of 10% to a low of 0% (Fig. 4). From 25.6 to 23.11 Ma, *R. minuta* has a stepwise increase in % abundance from 0% to 33%. There is one maximum and two

minima within the section. The maximum is found at 23.1 Ma with 33% abundance. The minima are found at 26.5 and 25.6 Ma with 0% abundance.

Hole U1406:

The taxon *R. minuta* also displays three abundance trends within the section of U1406 (Fig. 4). The first is a decreasing trend within the time frame of 26.7 to 25.6 Ma from a high of 55% to a low of 30%. The second trend is found within the interval 25.5 to 24.5 Ma, where *R. minuta* abundance appears to remain fairly constant. Within this interval of stability however, *R. minuta* has three minima and two maxima, with % abundance ranging from 32% to 40%. The third trend is a decrease in abundance within the interval of 24.5 to 23.2 Ma from a high of 40% to a low of 19%. *R. minuta* has two maxima within the section located at 26.7 Ma and 23.1 Ma of 55% and 47%, respectively (Fig. 4).

3.4 Biochronology:

This study identified 63 taxa, 4 of which represent standard bioevents using last appearance datums (LAD) and first appearance datums (FAD). Biostratigraphy of this paleolatitudinal transect is based on the CP zonation of Okada and Bukry, (1980) and the CNO zonation of Agnini et al. (2014; Fig. 5). The Agnini et al. (2014) CNO zonation divides the Late Oligocene into zones based on four biomarkers (Fig. 5). Ages of bioevents at Holes 926B, 563, and U1406 are calibrated using the geologic timescale of Gradstein et al. (2012). A list of nannofossil bioevents, samples, and depths for Holes 563, 926B, and U1406 can be found in Table 1.

Late Oligocene biostratigraphy - Hole 926B:

The section at Hole 926B contains moderately preserved common to abundant nannofossil assemblages. Samples 154-926B-51X-2 80-82 cm (473.3 m), and 154-926B-51X-4, 84-86 cm (476.4 m) mark the latest Oligocene with the LAD and FAD of *Sphenolithus delphix*. These samples represent the biozone of the upper part of CNO6 of Agnini et al. (2014) or Subzone CN1a of Okada and Bukry (1980) (Fig. 5). Biozone CNO5 or the CP19b Subzone is represented by the LAD of *Sphenolithus ciperoensis* and the LAD of S*phenolithus distentus* which is found in samples 154-926B-53X-CC, 6.5-8.5 cm (499.4 m) and 154-926B-61X-4, 36-38 cm (571 m) (Table 1).

Late Oligocene biostratigraphy – Site 628

The assemblages at Site 628 contain common to abundant, moderately preserved nannofossils; however, Sample 101-628-21H-3, 123-124 cm at 192.1 m is moderately preserved with rare to poor abundance. One biomarker was identified: the LAD of *S. distentus* at sample 101-628-23X-3, 8-9 cm (206.7 m) which marks the base of the CNO5 Biozone. Due to the disconformity at the top of this section, documented by Watkins and Verbeek (1988), identification of the top of *S. ciperoensis* could not be confirmed. The FAD of *S. ciperoensis* is used at the bottom of the section, based on the rare abundance as well as the identification of this biomarker by Moran and Watkins (1988).

Late Oligocene Biostratigraphy - Site 563:

The assemblages at Site 563 contains a common to abundant, moderately preserved nannofossils. Site 563 has six bioevents. The LAD and FAD of *S. delphix* of Biozone CNO6 are found in samples 82-563-16R-3, 114-115 cm and 82-563-16R-4, 96-97 cm, respectively (Table 1). The LAD of *S. ciperoensis* and *S. distentus*, which mark

the top and bottom boundaries for zone CNO5 are found in samples 82-563-17R-1, 117-118 cm and 82-563-18R-2, 2-3 cm, respectively. Finally, the FAD of *S. ciperoensis* and *S. distentus*, denoting the Biozone CNO4 are found in samples 82-563-18R-3, 49-50 cm and 82-563-19R-1, 120-121 cm, respectively (Table 1).

Late Oligocene Biostratigraphy – Hole U1406:

The section at Hole U1406 contain abundant, moderately preserved nannofossil assemblages. Three samples were identified as having poor preservation: 342-1406U-10H-5, 73-74, 342-1406U-12H-3, 133-134 cm, and 342-1406U-13H-4, 76-77 cm. Nannofossil abundance in Samples 12H-3 and 13H-4 are few, and Sample 10H-5 has abundant nannofossils.

Four bioevents were identified at Hole U1406. The LAD and FAD of *Sphenoltihus delphix* defining Biozone CNO6 were found in Samples 342-1406U-9H-6, 78-79 cm and 342-1406U-10H-5, 73-74 cm, respectively. The LAD of *S. ciperoensis* and *S. distentus*, denoting Biozone CNO5 where found in Samples 342-1406U-12H-2, 66-67 cm and 342-1406U-17R-1, 76-77 cm (Table 1).

3.5 Unitary Associations:

Biostratigraphic data from the six sites were used for quantitative analysis by the Unitary Association method (Guex, 1987) to examine the biostratigraphic relationships of the sites. The analysis produced 6 UAs (Fig. 6), with 9 maximal cliques and 5 contradictions. There are 28 horizons represented within the 6 UAs. These 6 UAs represent 6.9 m.y. of time from the Late Rupelian to Late Chattian, or the CNO4 – CNO6 zone of Agnini et al. (2014).

UA1:

Unitary Association One is characterized by the presence of *Pedinocyclus larvalis*, or *S. predistentus*. The LAD of *S. predistentus* also corresponds to the boundary between CNO4 and CNO5, with an age of 26.9 Ma. Site 563 is the only site where the LAD of *S. predistentus* (and UA1) is found. *P. larvalis* has an extremely rare abundance pattern, and the occurrence with *S. predistentus* should not be given biostratigraphic importance.

UA2:

Unitary Association two is characterized by the co-occurrence of *S. distentus* with any one of 15 taxa. Examination of these taxa indicate that (at least) 11 of these species (shaded gray in Figure 6) are known from older sediment at other localities. Their apparent first appearances in UA2 are the result of their paleoecological exclusion from UA1 at Site 563 (the only site with UA1 material in the study area). After eliminating these questionable occurrences, the first appearances in UA2 of *Sphenolithus avis, S. ciperoensis*, and *Triquetrorhabdulus challengeri* are probably real and useful. The presence of *S. distentus* and *S. ciperoensis* within this UA, marks the boundary between CNO5 and CNO6 at 24.43 Ma (Fig. 5).

UA3:

Unitary Association three is characterized by the occurrence of *R. hesslandii* and any one of 3 taxa: *Helicosphaera obliqua, Sphenolithus grandis*, and *Sphenolithus* sp. 1. Based upon the location of UA 3 in Site 563, the biostratigraphic placement is between the LAD of *S. distentus* at 26.84 Ma, and the LAD of *S. ciperoensis* at 24.43 Ma (Fig. 5).

UA4:

Unitary Association four is classified by the co-occurrence of 2 taxa: *S. calyculus* and *Dictyococcites stavensis*. The taxon *S. calyculus* has been used as a secondary bioevent for the Late Oligocene (Bergen et al., 2017). This places UA four within the Upper Late Oligocene, between the LAD of *S. ciperoensis* at 24.43 Ma and the FAD of *S. delphix* at 23.21 Ma. This zone is classified by CNO6 (Fig. 5).

UA5:

Unitary Association five is classified by the co-occurrence of *Chiasmolithus altus* or *Coccolithus eopelagicus*, and either *S. delphix* or *S. capricornutus*. The taxon *S. delphix* is a primary marker species, while *S. capricornutus* has been used as a secondary marker species (Bergen et al., 2017). The taxon of *C. altus* is used as a primary Late Oligocene marker species for the high latitudes of the Southern Ocean (Wise and Wind, 1983). UA 5 is within the FAD to LAD of *S. delphix* from 23.21 to 23.11 Ma which marks the upper CNO6 zone. The LAD of *S. delphix* marks the boundary between the Paleogene and Neogene or between CNO6 and CNM1 (Fig. 5).

UA6:

Unitary Association six is classified by the occurrence of *S. microdelphix* or *S. spinula*. Based on the species *S. microdelphix* and *S. spinula*, UA six can be placed just below the LAD of *S. delphix*, at 23.11 Ma, or just before the boundary between Biozones CNO6 and CNM1 (Fig. 5).

3.6 Rock Accumulation Rate:

An age versus depth analysis was conducted for Holes 926B, 628, 563, and U1406. These sites contain the temporal marker species necessary for correlation. Micropaleontologic data from foraminifera, radiolaria, and diatoms were included when available, as well as paleomagnetostratigraphic data. Due to a lack of biostratigraphic control at Holes 647A and 918D, a rock accumulation rate analysis could not be calculated.

Hole 926B:

Hole 926B rock accumulation rate was calculated using nannofossil and foraminiferal data (Fig. 7). Between the interval of the LAD and FAD of *S. delphix*, or from 23.1 to 23.2 Ma, the rock accumulation rate was 60 m/m.y. Between the interval of the FAD of *S. delphix* to the LAD of *S. ciperoensis*, from 23.2 to 24.4 Ma, the rock accumulation rate was 13.3 m/m.y. From the LAD of *S. ciperoensis* to the FAD of *Paragloborotalia pseudokugleri*, at 24.4 to 25.2 Ma, the rock accumulation rate was 10 m/m.y. Finally, from the FAD of *P. pseudokugleri* to the LAD of *S. distentus*, from 25.2 to 26.8 Ma, the rock accumulation rate was 40 m/m.y.

Site 628:

Site 628 has a truncated Upper Oligocene section, and as such, the rock accumulation rate analysis utilized foraminiferal markers. From the interval of the FAD of *Globigerinoides primordis* at 26.7 Ma, and the LAD of *Globigerina ciperoensis* at 23.6 Ma, Site 628 has an accumulation rate of 25.8 m/m.y. over 3.1 m.y. of time.

Site 563:

Site 563 rock accumulation rate was calculated using nannofossil markers. In the interval between the LAD of *S. distentus* and the LAD of *S. ciperoensis*, the accumulation rate is 5.1 m/m.y. In the interval between the LAD of *S. ciperoensis* and the LAD of *S. delphix*, the accumulation rate drops to 4 m/m.y.

Hole U1406:

Hole U1406 rock accumulation rates were calculated using nannofossil, radiolarian, and foraminiferal markers, as well as paleomagnetostratigraphy as seen in (Fig. 8). Between the interval between the LAD of *S. delphix* and the magnetostratigraphic chron C6Cn.2n, or 23.1 to 23.2 Ma, the rock accumulation rate was 150 m/m.y. From the interval between chron C6Cn.2n to chron C7n.1n, or from 23.2 to 23.9 Ma, the rock accumulation rate was 4.2 m/m.y. The interval of chron C7n.1n to chron C8r, or from 23.9 to 25.9 Ma, the rock accumulation rate was 21 m/m.y. Finally, from chron C8r to the LAD of *S. distentus*, or from 25.9 to 26.8 Ma, the rock accumulation rate was 8.8 m/m.y.

Summary of Results:

1.) Detrended Correspondence Analysis grouped samples along plot DCA1+2. The DCA1 and DCA2 axis are defined by environmental gradients which control the paleoecology and production of calcareous nannofossils within the North Atlantic (Fig. 2). In the DCA 1+2 plot, Site 563 is grouped separately from Sites 628, 926, and 1406.

2.) Shannon Diversity, shows average scores are higher for Site 563 and 926B and lower for U1406 (Fig. 3).

3.) The Unitary Associations Analysis produced 6 UAs, which are matched to paleogeographic sites (Fig. 6).

4.) Rock accumulation rate at Hole 926B is variable through time based on foraminiferal and nannofossil markers (Fig. 7), with the highest rate of accumulation of 40 m/m.y. from 25.2 to 26.8 Ma. Rock accumulation rate at Site 563 averaged 5-4 m/m.y. from 24.43 to 26.84 Ma. Rock accumulation rate at Hole U1406 was calculated using nannofossil, radiolarian, and foraminiferal markers, as well as paleomagnetostratigraphy as seen (Fig. 8). Highest rate of accumulation at this site was 21 m/m.y. within the interval of 23.9 to 25.9 Ma.

4.0 Discussion

4.1 Paleoecology Analysis:

Detrended Correspondence Analysis (DCA) indicates that much of the variance in the data matrix can be explained in terms of two gradients: DCA1 and DCA2. These gradients should correspond to significant ecological and oceanographic parameters that control the distribution of the calcareous nannofossil assemblages. The gradient that exerted the greatest control on the nannofossil distributions (DCA1) has a statistically highly significant Pearson correlation with the Temperature Index (TI) for the samples of $r = -0.92$, with a probability (p) that this relationship is actually random of a vanishingly small $p=3.8x10^{-68}$. This relationship (Fig. 9) strongly indicates that DCA1 is a reflection of temperature as the major factor in explaining the variance in the data matrix, and the relationship between the sites. The principle variables used to indicate warm conditions

in the TI also have high correlation coefficients to DCA1 with a r = -0.72 $p=2.7x10^{-21}$ for discoasters and an r = -0.70 $p=3.6x10^{20}$ for S*phenolithus*. The third variable of *C. pelagicus*, used to formulate the TI has a correlation coefficient of r =.028 p=.03 with the DC1 axis. As expected there is a higher correlation between *C. pelagicus* and the TI with an r = -0.37 $p=5.31x10^{-7}$. The lower R coefficient with the DC1 indicates that there may another paleoenvironmental factor controlling the production of *C. pelagicus* within this dataset.

The strong inverse correlation of the TI with DCA1 indicates that warmer temperatures (= high TI values) correspond with low DCA1 values. Examination of Figure 9 suggests a relatively continuous gradient from the warmest temperatures (upper left of graph) to the coolest (lower right of graph). Site 563 (orange on Fig. 9) which represents the center of the North Atlantic gyre, has generally the highest values of the TI and low DCA1 scores. Sites 628 (blue), 926 (black), and U1406 (red) represent the perimeter of the North Atlantic Gyre and show a trend of decreasing TI values and increasing DC1 scores. This suggests that the TI and DCA1 do not vary solely as a function of latitude but are controlled more directly by the oceanographic position of the site. The central North Atlantic gyre (536) has consistently warmer conditions than the gyre perimeter (628 & U1406) or the equatorial divergence (926). In a similar fashion, the northern Holes 918D (cyan) and 647A (green), located at 63˚ N and 53˚ N, respectively, are the reverse of what might be expected if latitude was the sole controlling feature. The higher latitude hole, 918D should correspond to a lower TI, rather than Hole 647A. The positions of Holes 647A and 918D in (Fig. 1) match modern day SST at the

Labrador Sea and the western coast of Iceland as can be seen in the NOAA SST map in (Fig. 10).

The Shannon Diversity index has a relatively high correlation with the DC1 scores with an $r = -0.68$ $p=8.9x10^{-24}$. This correlation is expected, as it is proven that a latitudinal increase directly corresponds to decreasing Shannon Diversity and paleoenvironmental stability (Bown et al. 2004).

The second major gradient indicated by Detrended Correspondence Analysis scores of DCA2 have a high correlation to the species *Reticulofenestra minuta* with an $r = -0.90$ $p=3.2x10^{-60}$. The high abundances of *R. minuta* (Fig. 11) correspond to lower DCA2 scores for Holes 926B (black) and U1406 (red). As illustrated in Figure 11, *R. minuta* percent abundance decreases with increasing DCA2 scores, which correspond to Sites 628 (blue), 647A (green), 918D (cyan), and 563 (orange). In order to constrain the DCA2 gradient and its association to *R. minuta*, the environmental preferences governing *R. minuta* production must be first analyzed.

In the study performed by Newsam et al. (2017), *R. minuta* was found have wide paleoecological tolerances with paleoenvironmental affinities for eutrophic cold-water conditions; however, Wade and Bown (2006) found that *R. minuta* could thrive under eutrophic warm water conditions such as those in the Mediterranean Sea during the Miocene. In this study, *R. minuta* has a low correlation to both the TI and the DC1 axis, with an $r = -0.22$ $p=.005$ for the TI, and an $r = 0.25$ $p=.001$ for the DC1. This indicates that *R. minuta* is not controlled principally by temperature.

Another possible environmental gradient controlling DC2 and *R. minuta* abundance could be sea surface salinity. Based upon modern day sea surface salinities per the CATDS Ocean Salinity Expert Center (CEC-OS, 2018), there is little change in sea surface salinity at the latitudinal locations of Holes 926B, U1406, and 563 (www.salinityremotesensing.ifremer.fr/sea-surface-salinity/salinity-distribution-at-the-ocean-surface). According to Zachos et al. (1994), Oligocene sea surface salinities were within 1.5 PSU of the modern day North Atlantic. An evaluation of Figure 4 reveals *R. minuta* abundances differ greatly between Holes U1406, 926B, and 563. This indicates that *R. minuta* is not principally controlled by sea surface salinity.

In general, *R. minuta* abundances are higher at sites with lower Shannon Diversity scores, or with more unstable paleoenvironmental conditions as is indicated by their statistically significant correlation ($r = -0.37$ $p=2.7x10^{-7}$). Sites such as 563 and 628, which have higher Shannon Diversity scores, and stable paleoenvironments, have correspondingly lower *R. minuta* percent abundance. The DC2 environmental gradient can therefore be related to nutrients, with lower DC2 scores corresponding to higher percentages of *R. minuta* (upper left corner of the graph), and higher DC2 scores to low *R. minuta* (lower right corner of the graph) (Fig. 11).

There is evidence of a span of volatility, possibly due to an increase in nutrients, within the Shannon Index at Site 563 which corresponds to an increasing trend in *R. minuta* percent abundance during the Late Oligocene. This volatility can be tracked through time from 26.8 to 23.8 Ma (Fig. 12). At Hole 926B, within the Late Oligocene an increase in the Shannon Index can be correlated to a decreasing trend in *R minuta* abundance through time. This trend can be tracked from 26.7 to 24.5 Ma (Fig. 13).

4.2 Biostratigraphy:

Unitary Associations: Biochronology

Comparison of the Unitary Associations to the zonation of Agnini et al. (2014) biochronology (Fig. 6, 5) indicates that although the two schemes are largely correlative, there are discrepancies between them. UA 1, defined by the LAD of *Sphenolithus predistentus*, correlates to the boundary between Biozones CNO4 and CNO5, so that Biozone CNO4 is equivalent to UA1. In the lower part of Biozone CNO5, the LAD of *Sphenolithus distentus* correlates to UA 2. The two schemes are similar, although Agnini et al. (2014) does not formally recognize the LAD of *S. distentus* as a zonal marker. UA 3 and UA 4, defined by the FAD of *Sphenolithus calyculus* cannot be correlated to the Agnini et al. (2014) biozones because that species is not present within their scheme. UA 5, defined by the base of *Sphenolithus delphix* correlates to late CNO6. Finally, UA 6 defined by the LAD of *S. delphix* and the presence of *S. microdelphix* correlates to the boundary between Biozones CNO6 and CNM1.

The boundary between Biozones CNO5 and CNO6 is defined by the LAD of *S. ciperoensis* in the Agnini et al. (2014) biochronology. Agnini et al. (2014) places the first occurrence of *S. delphix* at the top of CNO6; so that CNO6 is a gap zone between the LAD of *S. ciperoensis* and the FAD of *S. delphix*.

According to Bergen et al. (2017) the first occurrence (FO) of *S. delphix* occurs within the range of *S. ciperoensis*; which implies that *S. delphix* occurs lower in CNO6. To test the occurrence of *S. ciperoensis* and *S. delphix*; our study performed a detailed analysis of samples 154-926B- 54x-6, 76.5-78.5 cm, and 154-926B- 53x-4, 130-132 cm, which were chosen for relatively high counts of *S. ciperoensis*. A 400 FOV inspection of

these samples revealed the presence of *S. delphix* in rare to very rare abundances, concurrent with *S. ciperoensis*. *S. ciperoensis* ranges through the Unitary Associations 2-6.

Unitary Associations: Paleoecological Distribution:

The distribution of UAs in the North Atlantic shows a latitudinal change from equator to pole (Fig. 14). UA 1 is definitively found only at Site 563 in the gyre center, due to a deeper sampling for the site. UA 2 is definitive in the low to mid latitude of the North Atlantic, at Holes 926B, 628, 563, and U1406. UA 3 is definitive only with Sites 628 and 563 or the mid latitudes, and UA 4 is only found at Site 628. UA 5 is only differentiated at the low to mid latitude Sites U1406 and 563. UA 6 is only defined at Hole 926B. According to these distributions, there is less biostratigraphic resolution in high latitudes (647A and 918D) and at the equatorial divergence (926B). The best biostratigraphic resolution is located in the mid latitudes of the North Atlantic at Sites 628, 563, and U1406 (Fig. 14).

The distribution of UA 1-4 provides no definitive evidence of their existence in latitudes above 40° N (Fig. 14). The biochronology of Agnini et al. (2014) and Bergen et al. (2017) utilize sphenoliths that do not range into the high North Atlantic, and therefore these zonation schemes cannot be accurately applied to the Arctic and Sub-arctic zones. Neither zonation scheme utilizes the FAD of *Reticulofenestra hesslandii*, and therefore cannot define UA 3. (Fig. 14).

Unitary Association UA 6 is recognized only at Site 926, where it is separated from the underlying strata by a disconformity that includes all of UA 5. The gap between UA 3-4 and UA 6 at Site 926, or the absence of UA 5, (Fig. 14), is indicated by the

simultaneous FAD of *S. microdelphix, S. ciperoensis*, *S. delphix*, and *S. calyculus* in Sample 926B-54X-6W, 76-78 cm. At Holes 926B, *S. calyculus* should range lower in the section thus providing a definitive evidence of UA 5 within Hole 926B.

4.3 Rock Accumulation Rate Analysis: Holes 926B and U1406

The age versus depth models of Holes 926B and U1406 reveal decreasing rock accumulation rates, which reflect possible disconformities in the sections. The rock accumulation plot for Hole 926B has an increasing rate from 25 Ma to 23.1 Ma, with a plateau at the top of the section. This plateau correlates in time with the disconformity detected by the Unitary Associations analysis. Hole U1406, shows a shallowing and plateau of its rock accumulation rate located at chron C8r to the LAD of *S. distentus*, or from 25.9 to 26.8 Ma. This plateau correlated with the hiatus in Norris et al. (2014) which is placed at 26.5 to 28 Ma within the section.

5.0 Conclusions:

This study utilized a quantitative paleoecological analysis to constrain the paleoenvironmental controls governing calcareous nannofossil paleoproductivity and distribution in the late Oligocene North Atlantic Ocean. This distribution was then analyzed for its effect on the regional biostratigraphy in the North Atlantic Ocean.

1). DCA 1 is a temperature-related control on the paleoecology of the Late Oligocene North Atlantic Ocean. The DCA1 has a high correlation with the TI, and based on the distribution of high latitude sites, the thermal structure of the Late Oligocene North Atlantic was similar to the present day.

2.) The high correlations of Shannon Diversity, and DCA2 to the % abundance of *R. minuta* during the Late Oligocene indicate that it can be used as an indicator of paleoproductivity. The strong correlation with Shannon Diversity and DCA2 indicates that *R. minuta* is a principally eutrophic species, and DCA2 is a nutrient control on the paleoecology of the Late Oligocene.

3.) Comparison of the Unitary Associations to the zonation of Agnini et al. (2014) indicates biostratigraphic discrepancies. UA 3 and UA 4, defined by the base of *Sphenolithus calyculus* cannot be correlated to the Agnini et al. (2014) biozones. Testing the occurrences of *S. ciperoensis* and *S. delphix* based on the Bergen et al. (2017) scheme, reveals rare to very rare abundances of *S. delphix* concurrent with the range of *S. ciperoensis*.

4.) The zonations schemes of Bergen et al. (2017) and Agnini et al. (2014) cannot be accurately applied to the North Atlantic Ocean above 53° N. The best biostratigraphic resolution is confined to Sites 628, 563, and U1406 representing the mid latitudes. The distribution of UAs shows the least resolution in the High North latitudes (647A and 918D) or at the equatorial divergence (926B).

5.) The simultaneous FAD of *S. microdelphix, S. ciperoensis*, *S. delphix*, and *S. calyculus* at Hole 926B reveal a gap between UA 3-4 and UA6. The species *S. calyculus* should range lower in the section providing evidence of a UA5. This absence indicates a disconformity near the top of the section at Hole 926B.

6.) The rock accumulation rates of Holes 926B and U1406 reveal two disconformities within the respective sections. At Hole 926B there is a plateau which

corresponds to the UA 5 disconformity of the Unitary Associations analysis. Hole U1406 has a disconformity within chron C8r to the LAD of *S. distentus,* which correlates to the hiatus which Norris et al. (2014) noted at 26.5 to 28 Ma.

Taxonomic Notes:

Taxonomic notes include a list of all taxa discussed within this study, and a description of *Sphenolithus* sp. 1. Pictures of selected taxa mentioned in the text can be found in Figure 15.

List of taxa discussed in this study:

Chiasmolithus altus, Bukry and Percival, 1971

Coccolithus eopelagicus, (Bramlette & Riedel, 1954) Bramlette & Sullivan, 1961

Coccolithus pelagicus, (Wallich 1877) Schiller, 1930

Cyclocargolithus floridanus, (Roth & Hay, in Hay et al., 1967) Bukry, 1971

Dictyococcites stavensis, (Levin & Joerger, 1967) Varol, 1989

Heliocosphaera obliqua, Bramlette & Wilcoxon, 1967

Pedinocyclus gibbsiae, Bown & Dunkley Jones, 2012

Pedinocyclus larvalis, (Bukry & Bramlette, 1969) Loeblich & Tappan, 1973

Reticulofenestra daviesii, (Haq, 1968) Haq, 1971

Reticulofenestra hesslandii, (Haq,1966) Roth, 1970

Reticulofenestra minuta, Roth, 1970

Sphenolithus calyculus, Bukry, 1985

Sphenolithus capricornutus, Bukry & Percival 1971

Sphenolithus ciperoensis, Bramlette and Wilcoxon, 1967

Sphenolithus delphix, Bukry 1973

Sphenolithus distentus, (Martini, 1965) Bramlette & Wilcoxon, 1967

Sphenolithus grandis, Haq and Berggren, 1978

Sphenolithus microdelphix, Bergen & de Kaenel, in Bergen et al. 2017

Sphenolithus predistentus, Bramlette & Wilcoxon, 1967

Sphenolithus spinula, Bergen & de Kaenel, in Bergen et al. 2017

Sphenolithus sp. 1 is an informal name used to designate a small sphenolith less than 5 microns in length resembling the *Sphenolihus predistentus/ciperoensis* group.

Figures:

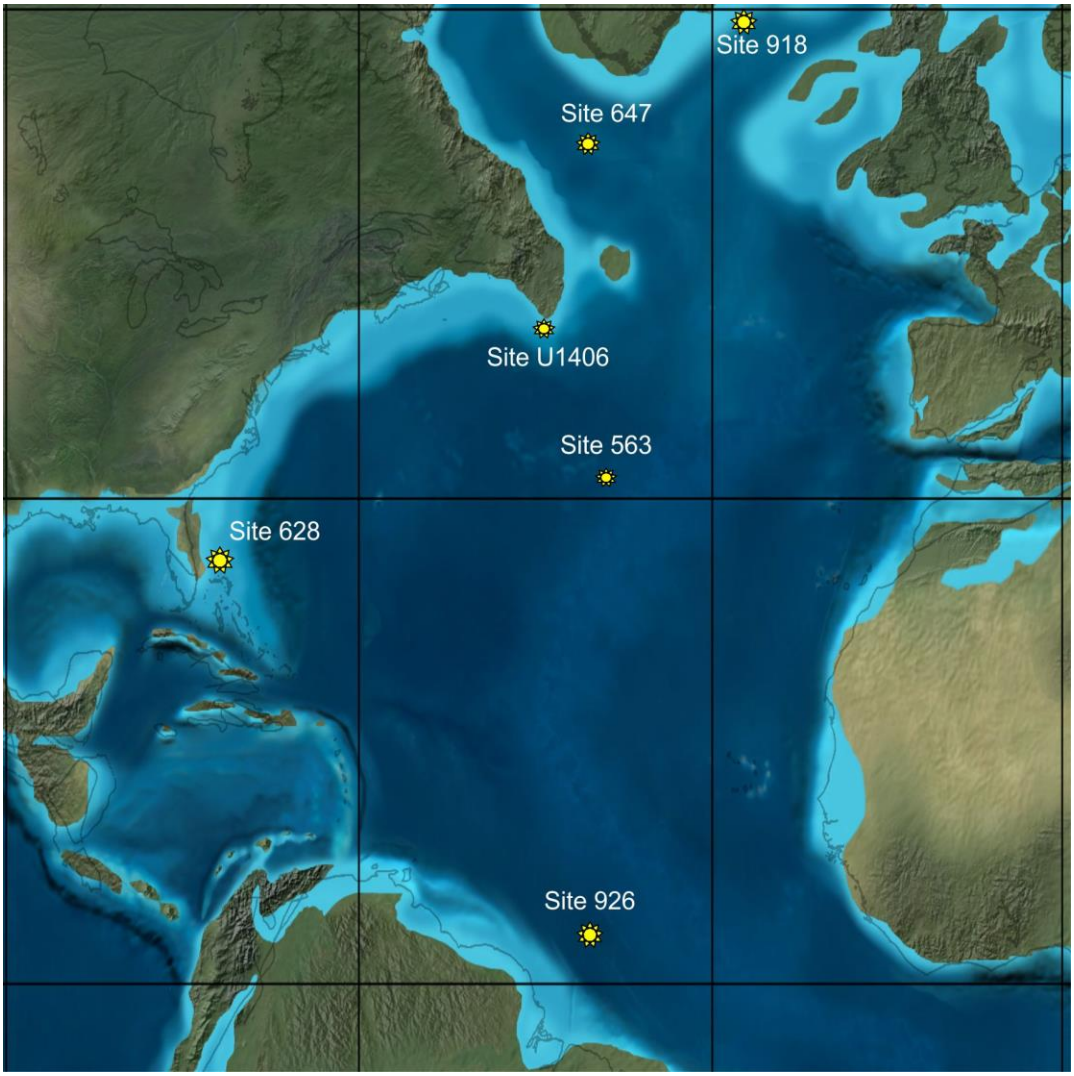

Figure 1: North Atlantic Ocean Locality Map. Map represents Early Oligocene configuration at 30 Ma. ODP Site 926B at 5^0 N, Site 628 at 27^0 N, Site 563 at 33^0N, Site U1406 at 42^0 N, Site 647A at 53^0 N, and Site 918D at 63^0 N. Map modified from Blakey Deep Time Maps.

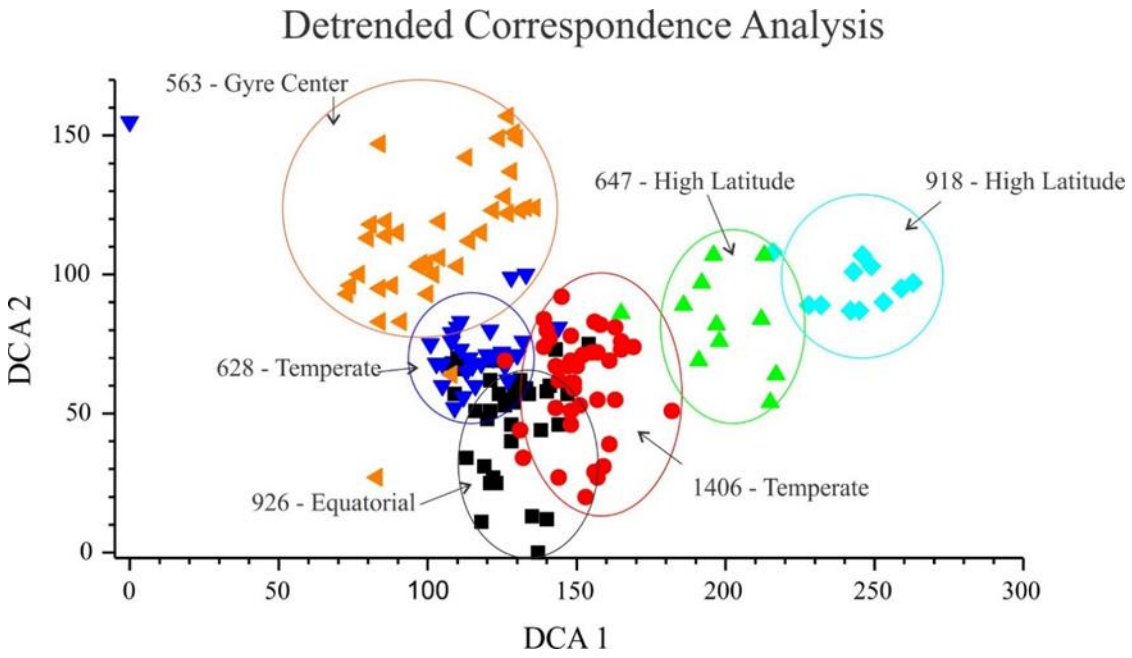

Figure 2: Plot of DC axis 1+2. Sites are categorized by color and shape. Site groupings are circled by their corresponding color. Holes 926B (black square), 628 (blue triangle), 563 (orange triangle), U1406 (red circle), 647A (green triangle), 918D (cyan diamond).

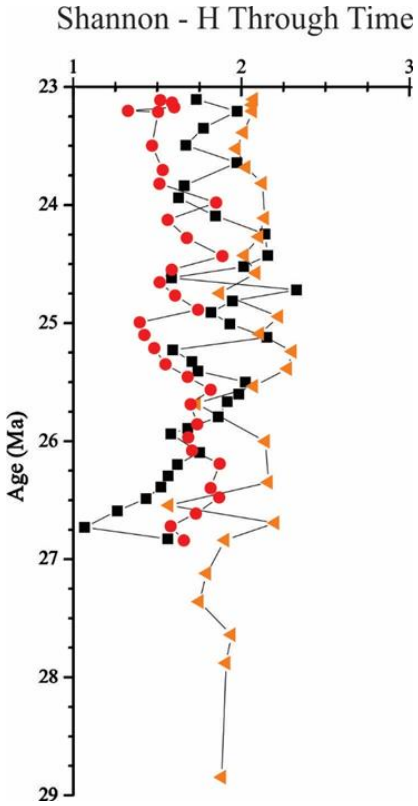

Figure 3: Shannon Diversity through time for Holes 926B, 563, and U1406. Hole 926B (black squares), Site 563 (orange triangle), and Site U1406 (red circle).

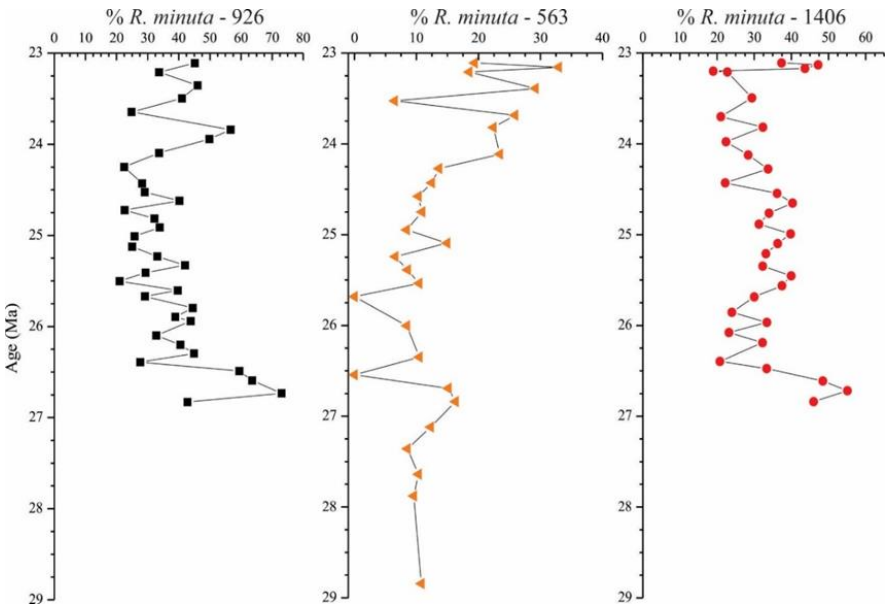

Figure 4: Percent abundance of *R. minuta* through time at Holes 926B, 563, and U1406.

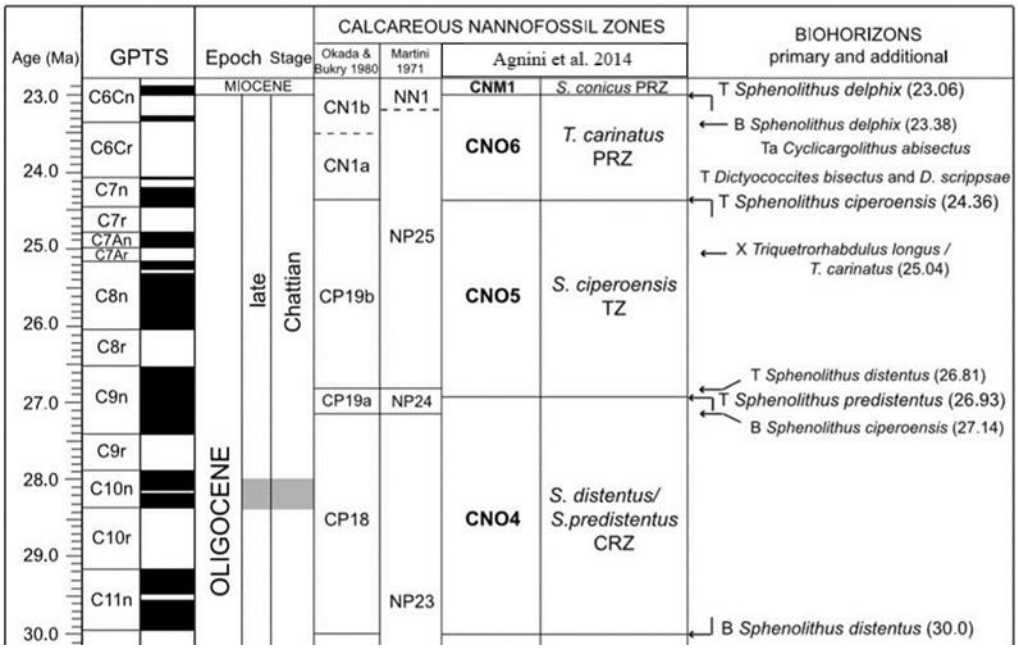

Figure 5: Biostratigraphy zonation chart modified from Agnini et al. (2014). This chart displays Late Oligocene biohorizons next to the Okada and Bukry (1980) and Martini (1971) zonations.

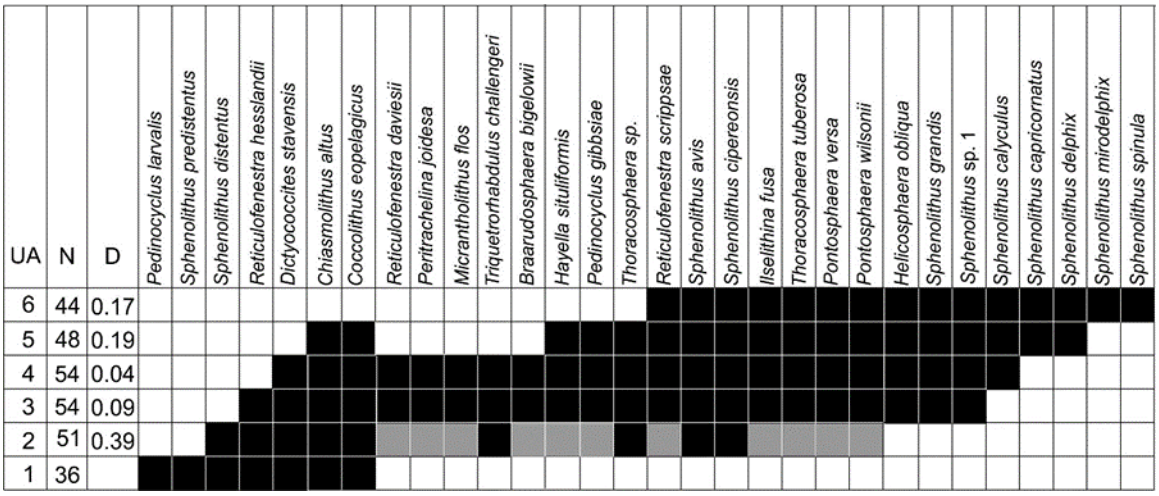

Figure 6: Unitary Associations of the dataset. 6 UAs, with sample (n). All species which range through the entire sequence have been removed from the solution. Black boxes mark the occurrence of taxa. Shaded boxes in UA 2 denote taxa that are known to range

lower in the assemblage. They appear as a first occurrence at UA 2 because they are not present in the assemblage at UA 1.

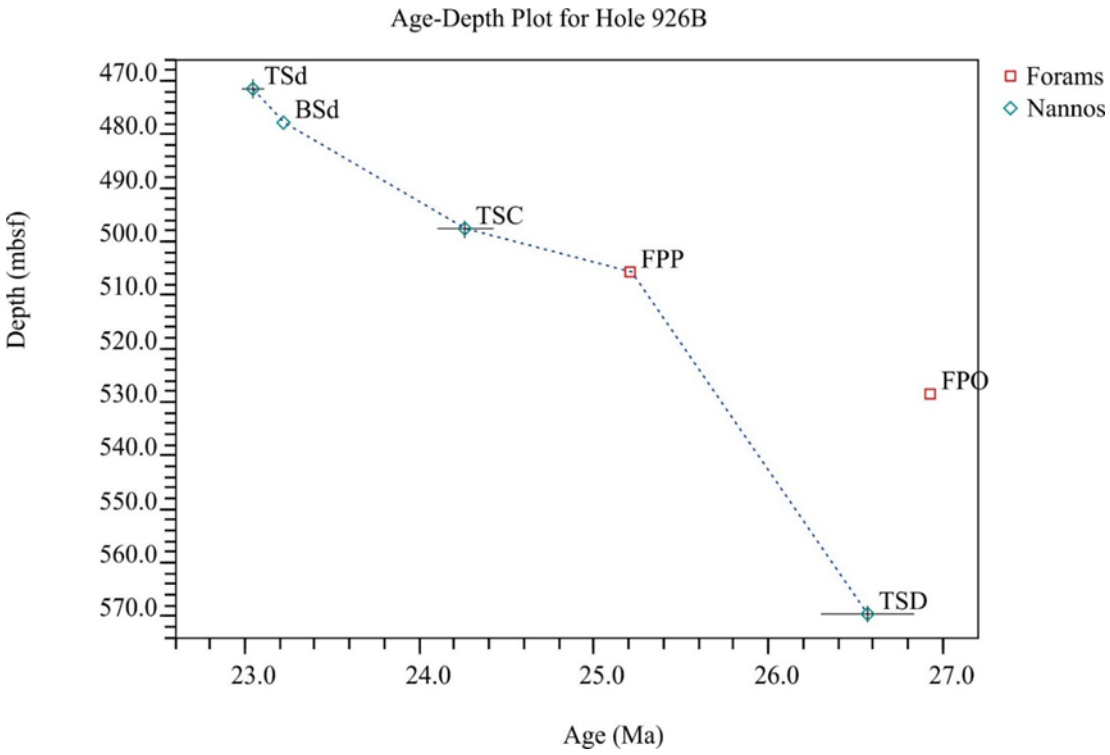

Figure 7: Age -Depth plot of Hole 926B. Model utilizes foraminifera and nannofossil markers. Data for this Age to Depth plot can be found in Table 3.

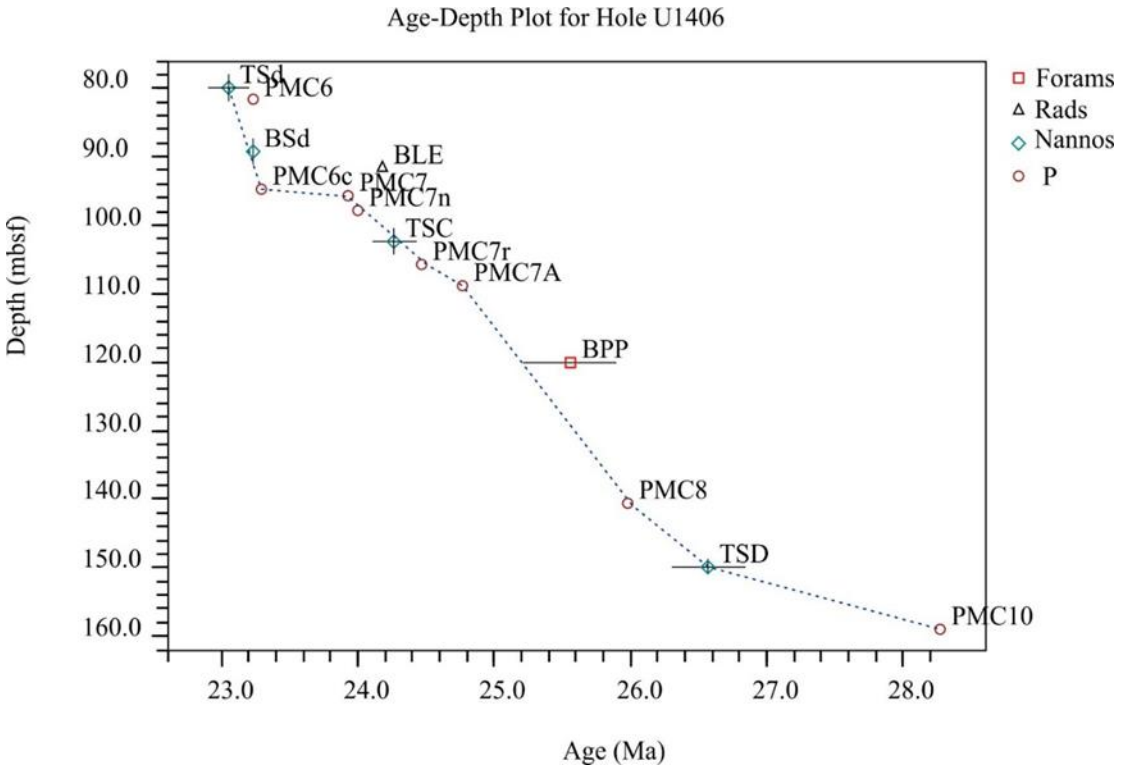

Figure 8: Age - Depth plot of Hole U1406. Model utilizes foraminiferal, nannofossil, and radiolarian marker species, and magnetostratigraphic chrons. A possible hiatus is located between PMC6c and PMC7. Data for this Age to Depth plot can be found in Table 4.

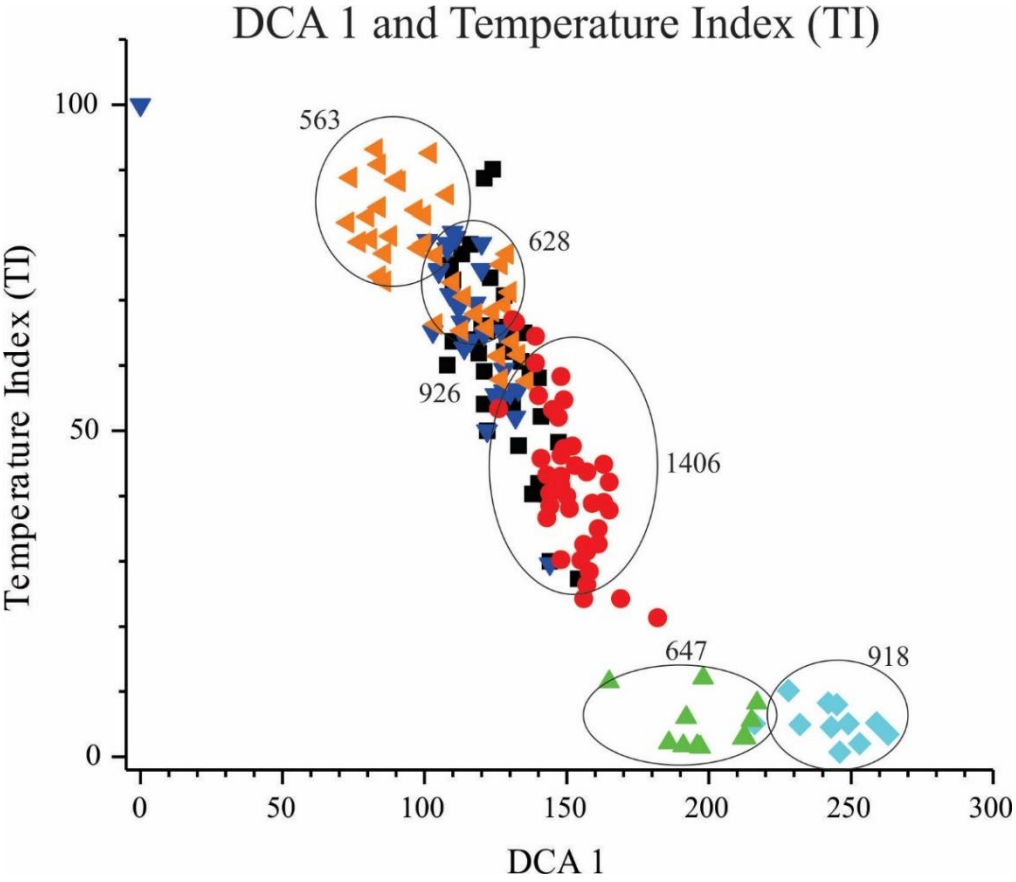

Figure 9: DC1 scores plotted to the temperature index by site. Site 926 (black squares), Site 628 (blue triangles), Site 563 (orange triangles), Site U1406 (red circles), Site 647 (green triangles), Site 918 (cyan diamonds).

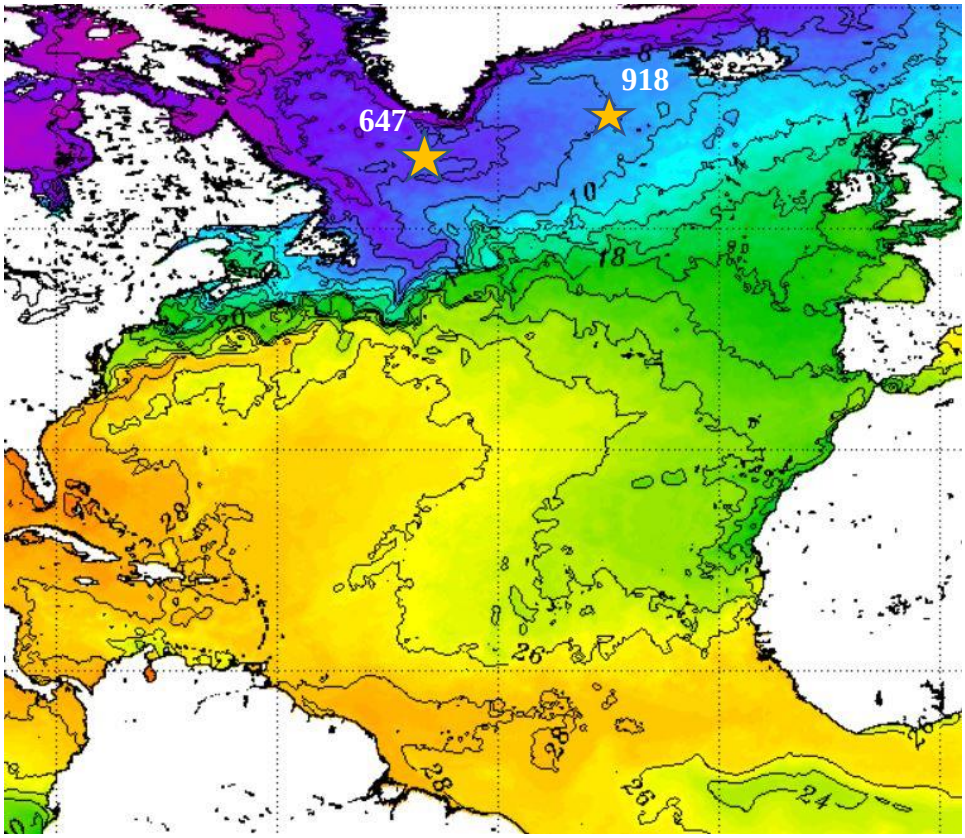

Figure 10: NOAA sea surface temperature contour map of the North Atlantic Ocean. The gold stars represent Sites 647 at 53˚, and 918 at 63˚.

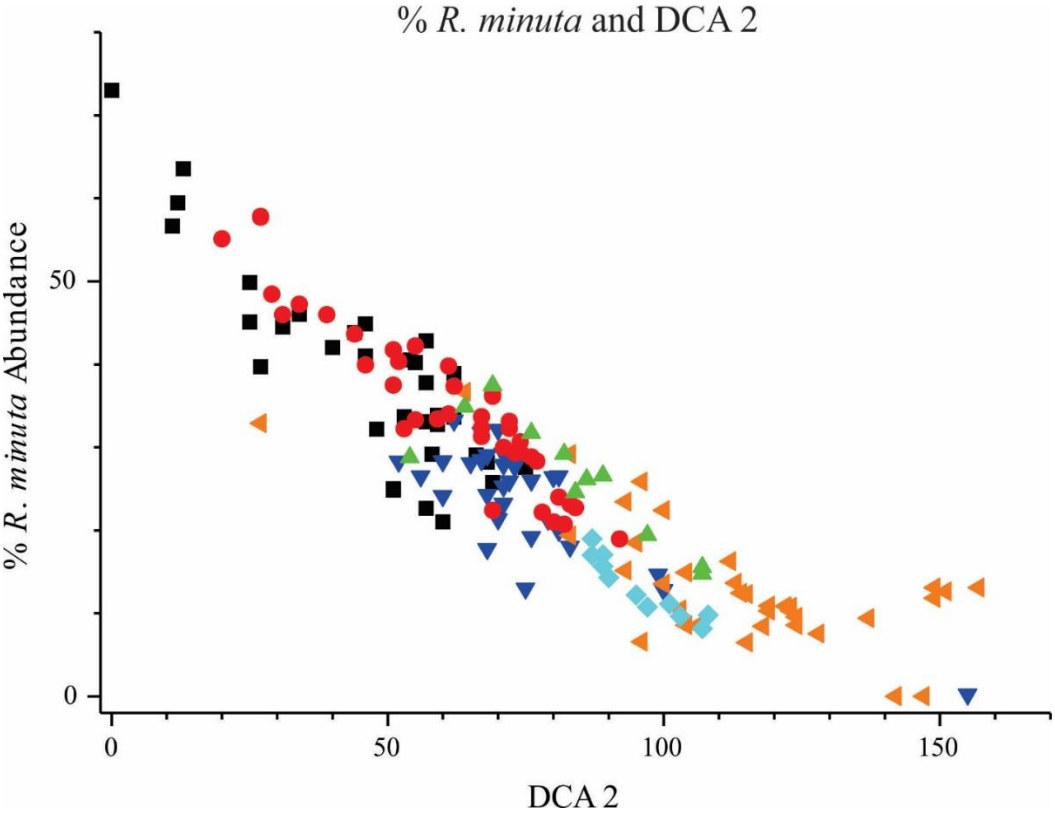

Figure 11: *R. minuta* and DCA2. High *R. minuta* percent abundances correlates to low DCA2 scores. Low *R. minuta* abundances correlate to high DCA2 scores. Site 926 (black squares), Site 628 (blue triangles), Site 563 (orange triangles), Site U1406 (red circles), Site 647 (green triangles), Site 918 (cyan diamonds).

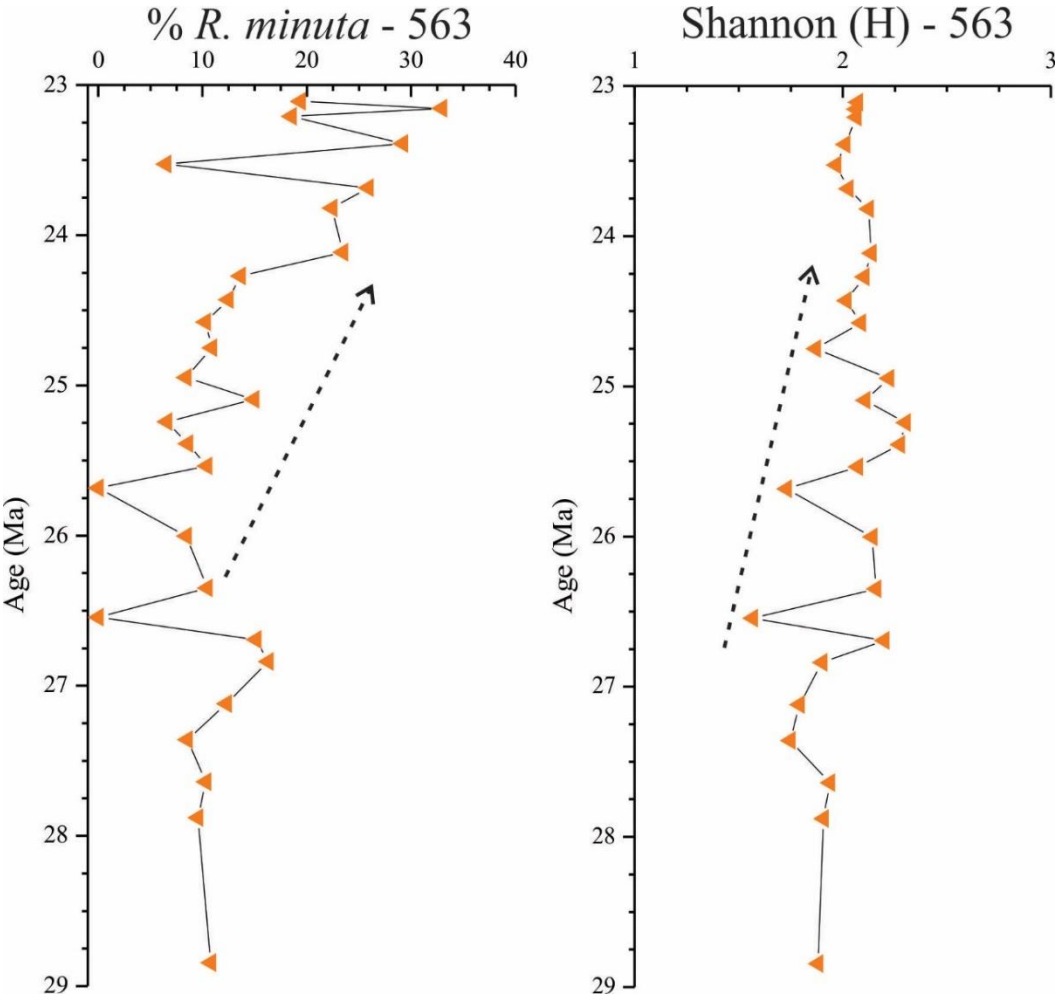

Figure 12: Percent abundance of *R. minuta* through time correlated to Shannon Diversity at Site 563. Lines denote *R. minuta* abundance increase during shifts in Shannon Diversity at Site 563.

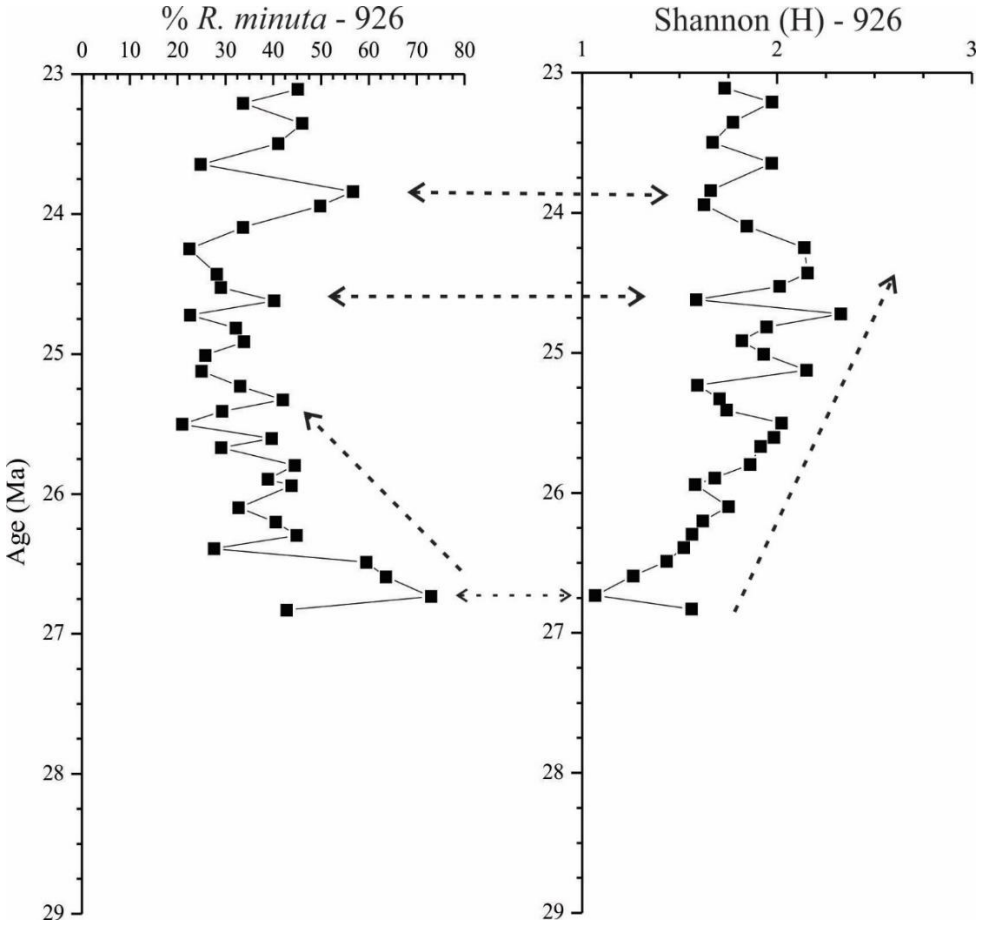

Figure 13: Percent abundance of *R. minuta* through time correlated to the Shannon Diversity of Hole 926B. Dashed lines correlate decrease in % *R. minuta* abundance through time to increasing Shannon Diversity through time. *R. minuta* minima and maxima are correlated to Shannon Diversity.

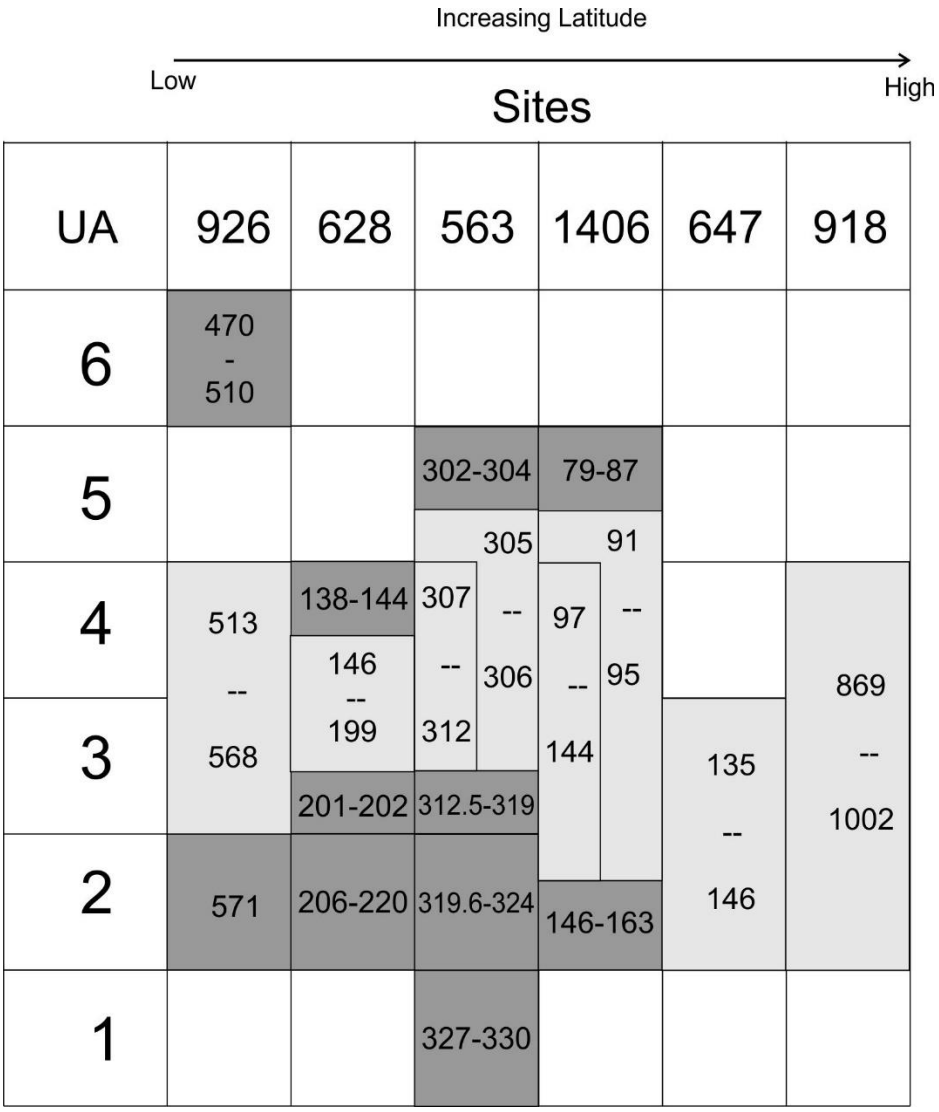

Figure 14: Unitary Associations divided up by samples and correlated by latitude. Block numbers indicate depth (m) where that UA is found within the site. The dark shaded blocks indicate where a UA is specifically defined. The light shaded blocks indicate where a UA ranges through a sample (e.g., Site 918 is defined by a range of UA 2 through UA 4).

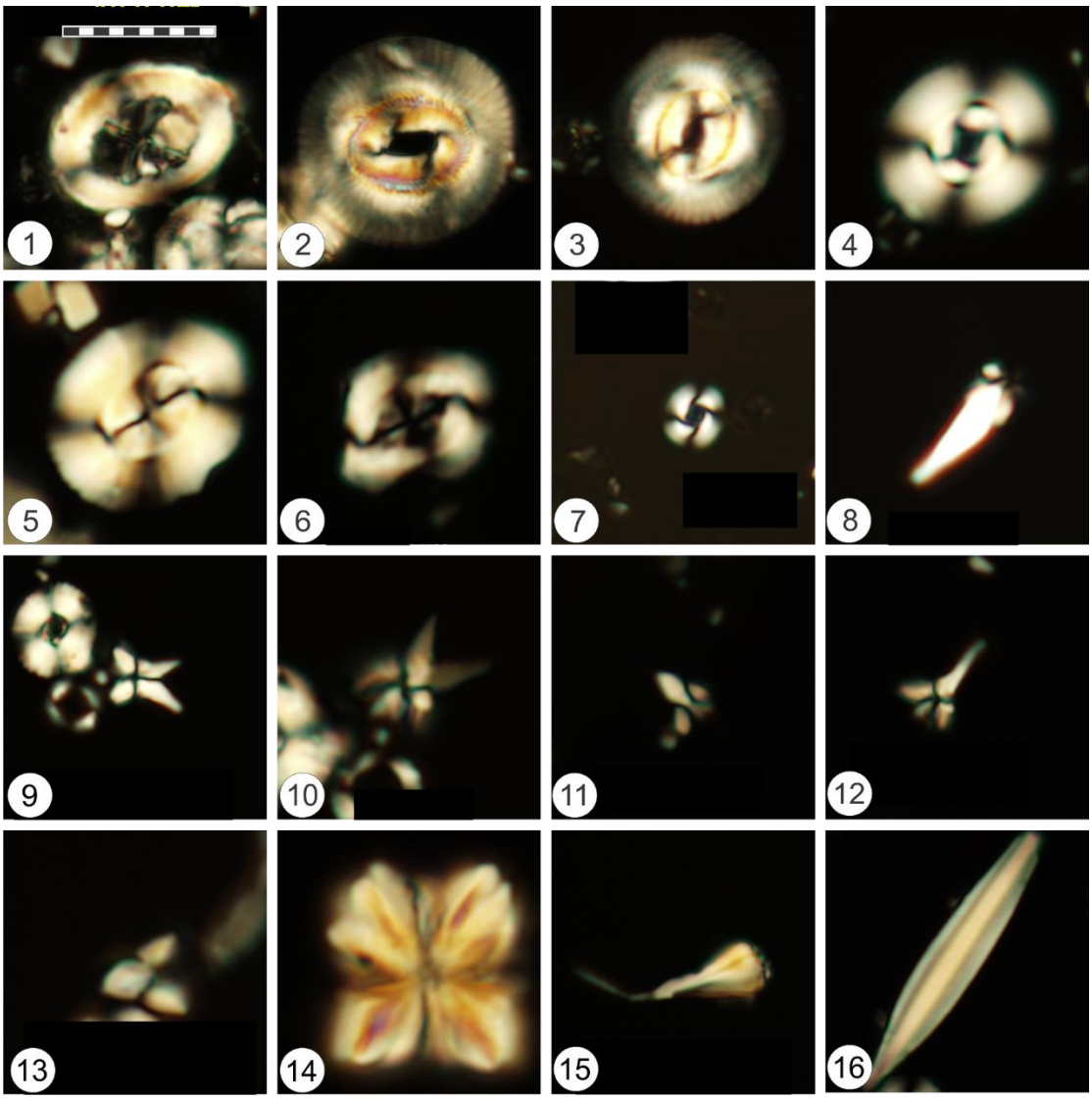

Figure 15: Images 1-15 were taken using crossed polarized light on an Olympus BX-51 light microscope under 1250x magnification. Scale found in picture 1 measures 10 microns. **1**. *Chiasmolithus altus*, **2**. *Coccolithus eopelagicus* **3**. *Coccolithus pelagicus* **4**. *Cyclicargolithus floridanus* **5**. *Dictyococcites stavensis* **6**. *Reticulofenestra daviesii*, **7**. *Reticulofenestra minuta* **8**. *Sphenolithus calyculus* **9 – 10** *Sphenolithus capricornutus* **11**. *Sphenolithus ciperoensis* **12**. *Sphenolithus delphix* **13**. *Sphenolithus distentus* **14**. *Sphenolithus grandis* **15**. *Sphenolithus predistentus* **16.** *Triquetrorhabdulus carinatus*

Tables:

Marker Taxa	**926, 3° N**	**628, 27° N**	**563, 33° N**	**U1406, 40° N**	**647, 53° N**	**918, 63° N**
LAD *S. delphix* (Tsd)	473.3 m		303.1 m	81 m		
FAD *S. delphix* (Bsd)	476.4 m		304.1 m	87.4 m		
LAD *S. ciperoensis* (TSC)	499.4 m		309.8 m	103.3 m		
LAD *S. distentus* (TSD)	571 m	206.7 m	319.6 m	148.8 m		
FAD *S. ciperoensis* (BSC)			321.6 m			
LAD *S. predistentus* (TSP)						
FAD *S. distentus* (BSD)			327.5 m			

Table 1: Bioevents identified at their approximate depth for each site. No sphenolith markers were fund for Sites 647 and 918. Bioevents are labeled using their identification code corresponding to the Age-Depth Plots in table 3 and 4.

	Temperature Index										
Depth m	**926B (Ti)**	**Depth m**	**628 (Ti)**	**Depth m**	**563 (Ti)**	**Depth m**	**U1406 (Ti)**	**Depth m**	**647A (Ti)**	**Depth m**	**918D (Ti)**
469.9	90.11	137.90	65.26	301.80	92.57	78.90	40.43	135.70	5.10	869.00	1.73
473.3	88.73	139.80	70.90	302.50	86.23	81.00	38.52	136.00	8.26	871.00	2.19
476.4	65.94	141.80	63.52	303.10	88.24	82.30	66.67	137.00	5.24	879.40	11.51
479.1	77.10	143.70	77.90	303.70	93.18	84.80	67.03	137.60	4.55	983.20	12.14
481.8	62.16	146.70	78.72	304.40	90.84	86.80	53.26	137.90	3.45	992.90	1.51
484.6	78.63	147.90	80.39	305.20	84.23	87.40	60.42	138.40	0.74	993.50	5.60
487.5	64.00	149.80	79.65	305.80	88.41	91.10	64.47	138.70	10.19	994.40	8.25
490.2	73.49	151.40	78.76	306.50	88.81	93.80	55.38	139.00	4.96	995.10	2.88
493.1	59.09	153.70	66.67	307.10	78.93	95.30	36.67	145.20	5.06	995.70	2.95
496	63.73	155.60	74.39	308.40	81.91	97.40	53.40	145.50	2.00	997.10	6.04
499.4	60.09	158.40	70.00	309.10	82.83	99.30	45.79	146.10	8.04	1002.20	1.73
502.2	73.15	160.20	63.83	309.80	77.20	101.30	52.08				
505.1	70.77	162.10	64.84	310.40	72.90	103.30	46.22				
508.1	75.43	164.40	65.22	311.10	66.33	105.50	32.67				
510.9	66.10	169.60	68.87	311.90	79.38	107.50	43.21				
513.8	55.24	171.50	62.70	312.50	78.03	109.60	54.76				
516.7	65.28	173.50	79.17	313.10	79.85	111.90	40.00				
520.1	54.07	189.80	55.56	313.70	78.66	113.90	41.67				
523.3	48.24	192.10	100.00	314.30	72.73	115.90	30.25				
526.2	55.56	193.60	54.26	314.90	73.67	118.00	26.44				
528.6	40.24	195.30	52.08	316.20	76.86	120.60	30.21				
531.4	52.21	197.70	55.81	317.60	83.88	122.60	43.02				
534.4	50.00	199.50	74.69	318.40	65.34	124.70	58.33				
536.4	41.94	201.40	56.10	319.00	83.02	127.00	47.67				
540.2	61.87	202.60	59.44	319.60	70.56	130.20	44.90				
543.1	54.19	206.70	69.54	320.30	67.87	132.30	47.30				
544.5	40.32	208.50	74.68	320.90	61.62	134.40	32.61				
549.2	47.71	210.50	29.60	321.60	65.81	136.50	38.10				
552.2	64.75	218.30	56.30	322.20	57.62	140.40	28.43				
555.1	30.00	220.00	50.00	322.80	63.68	141.90	31.52				
557.9	27.34			323.40	61.47	144.50	24.24				
560.8	58.11			324.30	57.89	146.50	44.64				
563.9	65.00			326.80	68.24	148.80	38.89				
568.1	59.38			327.50	75.51	150.90	35.00				
571	60.69			329.00	77.09	152.90	43.68				
				3297.00	71.24	154.90	21.36				
				330.60	69.30	157.20	24.24				
						159.30	42.11				
						161.40	37.84				
						163.60	39.02				

Table 2: Temperature index of sea surface in the North Atlantic Ocean, matched to sample depth. Index is an arbitrary scale of 0-100 scorings, where 0 is the coldest and 100 is the hottest. Derived from (TI) formula, modified from (Watkins and Self-Trail, 2005, Villa et al. 2014).

926B	2	1/27/2018	BTH			
Group	Event	Plotcode	Young Age	Old Age	Top Depth	Bottom Depth
N	LAD S. delphix	TSd	22.98	23.11	469.9	473.3
N	FAD S. delphix	BSd	23.21	23.24	476.4	479.1
N	LAD S. ciperoensis	TSC	24.1	24.43	496	499.4
N	LAD S. distentus	TSD	26.3	26.84	568.1	571
F	FAD P. pseudokugleri	FPP	25.21	25.21	505.86	
F	LAD P. opima	FPO	26.93	26.93		528.5

Table 3: Age - Depth data for the Hole 926B rock accumulation rate analysis in Fig. 4.

U1406	2	1/27/2018	BTH			
Group	Event	Plotcode	Young Age	Old Age	Top Depth	Bottom Depth
N	LAD S. delphix	TSd	22.98	23.11	78.9	81
N	FAD S. delphix	BSd	23.21	23.24	87.4	91.1
N	LAD S. ciperoensis	TSC	24.1	24.43	101.3	103.3
N	LAD S. distentus	TSD	26.3	26.84	148.8	150.9
F	FAD P. pseudokugleri	BPP	25.21	25.9	119.98	
R	FAD L. elongata	BLE	24.18	24.18	91.65	
P	C6Cn.2n	PMC6	23.23	23.23	81.11	82.21
P	C6Cr	PMC6c	23.29	23.29	94.6	94.83
P	C7n.1n	PMC7	23.92	23.92	95.68	95.83
P	C7n.1r	PMC7n	24	24	97.53	97.95
P	C7r	PMC7r	24.47	24.47	105.58	105.83
P	C7An	PMC7A	24.76	24.76	108.58	108.9
P	C8r	PMC8	25.98	25.98	140.38	140.8
P	C10r	PMC10	28.27	28.27	158.94	159.04

Table 4: Age - Depth data for the Site U1406 rock accumulation rate analysis in Fig. 5.

References:

Agnini, C., Fornaciari, E., Raffi, I., Catanzariti, R., Pälike, H., Backman, J., & Rio, D. (2014). Biozonation and biochronology of Paleogene calcareous nannofossils from low and middle latitudes. Newsletters on Stratigraphy, 47(2), 131-181.

Baldauf, J. G., Clement, B. G., Aksu, A. E., de Vernal, A., Firth, J. V., Hall, F., & Monjanel, A. L. (1989). Magnetostratigraphic and biostratigraphic synthesis of ocean drilling program Leg 105: Labrador Sea and Baffin Bay. In Proceedings of the Ocean Drilling Program: Scientific Results (Vol. 105, pp. 935-956).

Bergen, J.A.; de Kaenel, E.; Blair, S.A.; Boesiger, T.M. & Browning, E., (2017). Oligocene-Pliocene taxonomy and stratigraphy of the genus Sphenolithus in the circum-North Atlantic Basin: Gulf of Mexico and ODP Leg 154. Journal of Nannoplankton Research, 37(2-3): 77-112.

Blaj, T., Backman, J., & Raffi, I. (2009). Late Eocene to Oligocene preservation history and biochronology of calcareous nannofossils from paleo-equatorial Pacific Ocean sediments. *Rivista Italiana di Paleontologia e Stratigrafia (Research In Paleontology and Stratigraphy)*, *115*(1).

Bown, P. R., Lees, J. A., & Young, J. R. (2004). Calcareous nannoplankton evolution and diversity through time. In *Coccolithophores* (pp. 481-508). Springer, Berlin, Heidelberg.

Bown, P. R., & Dunkley-Jones, T. (2012). Calcareous nannofossils from the Paleogene equatorial Pacific (IODP Expedition 320 Sites U1331-1334). *Journal of Nannoplankton Research*, Res. 32 (2) (pp3-51).

CATDS, Salinity Expert Center (2018). [Graphic illustration of Salinity Distribution at the Ocean Surface, 2005]. Received from http://www.salinityremotesensing.ifremer.fr/sea-surface-salinity/salinity-distribution-at-the-ocean-surface.

Chang, Y. M. (1967). Accuracy of fossil percentage estimation. *Journal of Paleontology*, 500-502.

Cramer, B. S., Toggweiler, J. R., Wright, J. D., Katz, M. E., & Miller, K. G. (2009). Ocean overturning since the Late Cretaceous: Inferences from a new benthic foraminiferal isotope compilation. *Paleoceanography and Paleoclimatology*, *24*(4).

Curry, W. B., Shackleton, N. J., & Richter, C. (1995). Leg 154. Synthesis. Proceedings ODP, Initial Reports, 154, 421-442.

Firth, J. V. (1989). Eocene and Oligocene calcareous nannofossils from the Labrador Sea, ODP Leg 105. In Proceedings of the Ocean Drilling Program, Scientific Results (Vol. 105, pp. 263-286).

Frankignoul, C., de Coëtlogon, G., Joyce, T. M., & Dong, S. (2001). Gulf Streamvariability and ocean–atmosphere interactions. Journal of Physical Oceanography, 31(12), 3516-3529.

Geisen, M., Bollmann, J., Herrle, J. O., Mutterlose, J., & Young, J. R. (1999). Calibration of the random settling technique for calculation of absolute abundances of calcareous nannoplankton. Micropaleontology, 437-442.

Gibbs, S., Shackleton, N., & Young, J. (2004). Orbitally forced climate signals in mid-Pliocene nannofossil assemblages. Marine Micropaleontology, 51(1), 39-56.

Gradstein, F. M. (2012). Introduction. In The geologic time scale, Elsevier BV.

Guex, J. (1987), *Correlations Biochronoloiques et Associationa Unitaires*, Presses Polytechniques Romandes.

Hammer, Ø., Harper, D. A. T., & Ryan, P. D. (2001). PAST-palaeontological statistics, ver. 1.89. *Palaeontol electron*, *4*(1), 1-9.

Heydt, A., & Dijkstra, H. A. (2006). Effect of ocean gateways on the global ocean circulation in the late Oligocene and early Miocene. *Paleoceanography*, *21*(1).

Japsen, P., Green, P. F., & Chalmers, J. A. (2005). Separation of Palaeogene and Neogene uplift on Nuussuaq, West Greenland. *Journal of the Geological Society*, *162*(2), 299-314.

Japsen, P., Bonow, J. M., Green, P. F., Chalmers, J. A., & Lidmar-Bergström, K. (2006). Elevated, passive continental margins: Long-term highs or Neogene uplifts? New evidence from West Greenland. *Earth and Planetary Science Letters*, *248*(1-2), 330-339.

Kennett, J. P. (1982). Marine Geology, Prentice Hall, 657 - 658 pp.

Livermore, R., Nankivell, A., Eagles, G., & Morris, P. (2005). Paleogene opening of Drake passage. *Earth and Planetary Science Letters*, *236*(1-2), 459-470.

Martini, E. (1971). Standard Tertiary and Quaternary calcareous nannoplankton zonation. In *Proc. II Planktonic Conference, Roma 1970, Roma, Tecnoscienza* (Vol. 2, pp. 739-785).

Miller, K. G., Aubry, M. P., Khan, M. J., Melillo, A. J., Kent, D. V., & Berggren, W. A. (1985). Oligocene-Miocene biostratigraphy, magnetostratigraphy, and isotopic stratigraphy of the western North Atlantic. Geology, 13(4), 257-261.

Miller, K. G., Fairbanks, R. G., & Mountain, G. S. (1987). Tertiary oxygen isotope synthesis, sea level history, and continental margin erosion. Paleoceanography, 2(1), 1-19.

Montes, C., Bayona, G., Cardona, A., Buchs, D. M., Silva, C. A., Morón, S., & Valencia, V. (2012). Arc- continent collision and orocline formation: Closing of the Central American seaway. Journal of Geophysical Research: Solid Earth, 117(B4).

Moran, M. J., & Watkins, D. K. (1988). Oligocene calcareous-nannofossil biostratigraphy from Leg 101, Site 628, Little Bahama Bank slope.

Newsam, C., Bown, P. R., Wade, B. S., & Jones, H. L. (2017). Muted calcareous nannoplankton response at the Middle/Late Eocene Turnover event in the western North Atlantic Ocean. Newsletters on Stratigraphy, 50(3), 297-309.

Norris, R. D., Wilson, P. A., & Blum, P. and the Expedition 342 Scientists (2014). Proceedings IODP, 342. College Station, TX (Integrated Ocean Drilling Program). doi:10.224/iodp.proc.342.2014

Okada, H., & Bukry, D. (1980). Supplementary modification and introduction of code numbers to the low-latitude coccolith biostratigraphic zonation (Bukry, 1973; 1975). Marine Micropaleontology, 5, 321-325.

Parker, M. E. (1985). Calcareous nannofossil of Deep Sea Drilling Project Sites 558 and 563, North Atlantic Ocean: biostratigraphy and the distribution of Braarudosphaerids. *Init. Repts. DSDP*, *82*, 559-589.

Pekar, S. F., Christie-Blick, N., Kominz, M. A., & Miller, K. G. (2002). Calibration between eustatic estimates from backstripping and oxygen isotopic records for the Oligocene. Geology, 30(10), 903-906.

Pekar, S. F., DeConto, R. M., & Harwood, D. M. (2006). Resolving a late Oligocene conundrum: deep-sea warming and Antarctic glaciation. Palaeogeography, Palaeoclimatology, Palaeoecology, 231(1-2), 29-40.

Pfuhl, H. A., & McCave, I. N. (2005). Evidence for late Oligocene establishment of theAntarctic Circumpolar Current. Earth and Planetary Science Letters, 235(3), 715-728.

Piasecki, S. (2003). Neogene dinoflagellate cysts from Davis strait, offshore West Greenland. *Marine and Petroleum Geology*, *20*(9), 1075-1088.

Pinet, P. R., & Popenoe, P. (1985). A scenario of Mesozoic-Cenozoic ocean circulation over the Blake Plateau and its environs. Geological Society of America Bulletin, 96(5), 618-626.

Reuter, M., Piller, W. E., Harzhauser, M., Mandic, O., Berning, B., Rögl, F., & Hamedani, A. (2009). The Oligo-/Miocene Qom Formation (Iran): evidence for an early Burdigalian restriction of the Tethyan Seaway and closure of its Iranian gateways. *International Journal of Earth Sciences*, *98*(3), 627-650.

Scher, H. D., & Martin, E. E. (2006). Timing and climatic consequences of the opening of Drake Passage. Science, 312(5772), 428-430.

Shackleton, N. J., Crowhurst, S. J., Weedon, G. P., & Laskar, J. (1999). Astronomical calibration of Oligocene--Miocene time. *Philosophical Transactions of the Royal Society of London A: Mathematical, Physical and Engineering Sciences*, *357*(1757), 1907-1929.

Stoker, M. S., Nielsen, T., Van Weering, T. C. E., & Kuijpers, A. (2002). Towards an understanding of the Neogene tectonostratigraphic framework of the NE Atlantic margin between Ireland and the Faroe Islands. Marine Geology, 188(1-2), 233-248.

Villa, G., Fioroni, C., Persico, D., Roberts, A. P., & Florindo, F. (2014). Middle Eoceneto Late Oligocene Antarctic glaciation/deglaciation and Southern Ocean productivity. Paleoceanography and Paleoclimatology, 29(3), 223-237.

Wade, B. S., & Bown, P. R. (2006). Calcareous nannofossils in extreme environments: the Messinian salinity crisis, Polemi Basin, Cyprus. Palaeogeography, Palaeoclimatology, Palaeoecology, 233(3), 271-286.

Watkins, D. K., & Bowdler, J. L. (1984). Cretaceous calcareous nannofossils from deep sea drilling project Leg 77, southeast Gulf of Mexico.

Watkins, D. K., & Verbeek, J. W. (1988). Calcareous nannofossil biostratigraphy from Leg 101, northern Bahamas.

Watkins, D. K., & Self-Trail, J. M. (2005). Calcareous nannofossil evidence for the existence of the Gulf Stream during the late Maastrichtian. *Paleoceanography*, *20*(3).

Wei, W. (1998) Calcareous nannofossils from the southeast Greenland margin: biostratigraphy and paleoceanography. *Proceedings of the Ocean Drilling Program*, Vol. 152.

Wise, S. W., & Wind, F. H. (1983). Mesozoic and Cenozoic calcareous nannofossils recovered by DSDP Leg 71 in the Falkland Plateau region, Southwest Atlantic Ocean. *Initial Reports of the Deep Sea Drilling Project*, *71*, 481-550.

Zachos, J. C., Stott, L. D., & Lohmann, K. C. (1994). Evolution of early Cenozoic marine temperatures. *Paleoceanography*, *9*(2), 353-387.